

1 Neuronal dystroglycan is necessary for formation and maintenance  
2 of functional CCK-positive basket terminals on pyramidal cells

3 Dystroglycan function at CCK-positive terminals

4 **Simon Früh<sup>1,5</sup>, Jennifer Romanos<sup>1,5</sup>, Patrizia Panzanelli<sup>2</sup>, Daniela Bürgisser<sup>3</sup>,**  
5 **Shiva K. Tyagarajan<sup>1,5</sup>, Kevin P. Campbell<sup>4</sup>, Mirko Santello<sup>1,5</sup>, Jean-Marc**  
6 **Fritschy<sup>1,5</sup>**

7 <sup>1</sup>Institute of Pharmacology and Toxicology, University of Zurich, 8057 Zurich, Switzerland <sup>2</sup>Department  
8 of Neuroscience Rita Levi Montalcini, University of Turin, 10124 Turin, Italy <sup>3</sup>ETH Zurich, 8092 Zurich,  
9 Switzerland <sup>4</sup>Howard Hughes Medical Institute, Department of Molecular Physiology and Biophysics,  
10 Department of Neurology, The University of Iowa Roy J. and Lucille A. Carver College of Medicine,  
11 Iowa City, Iowa 52242, USA <sup>5</sup>Neuroscience Center Zurich, University of Zurich and ETH Zurich, 8057  
12 Zurich, Switzerland

13 Corresponding author: Jean-Marc Fritschy, Institute of Pharmacology and Toxicology,  
14 Winterthurerstrasse 190, 8057 Zurich, Switzerland, fritschy@pharma.uzh.ch

15

16 Number of pages: 32

17 Number of figures: 11

18 Number of words, abstract: 240 introduction: 649 discussion: 1464

19

20 Conflict of interest: The authors declare no competing financial interests.

21

22 Acknowledgements: This work was supported by a University of Zurich Forschungskredit  
23 grant to SF, the Swiss National Science Foundation (grant 310030\_146120 to JMF) and a  
24 Paul D. Wellstone Muscular Dystrophy Cooperative Research Center grant (1U54NS053672  
25 to KPC). KPC is an investigator of the Howard Hughes Medical Institute. We thank Prof.

26 Peter Scheiffele and Prof. Stephan Neuhaus for scientific discussion and Dr. Tatjana  
27 Haenggi and Cornelia Schwerdel for genotyping.

28

29 **Distinct types of GABAergic interneurons target different subcellular domains of**  
30 **pyramidal cells, thereby shaping pyramidal cell activity patterns. Whether the**  
31 **presynaptic heterogeneity of GABAergic innervation is mirrored by specific**  
32 **postsynaptic factors is largely unexplored. Here we show that dystroglycan, a protein**  
33 **responsible for the majority of congenital muscular dystrophies when dysfunctional,**  
34 **has a function at postsynaptic sites restricted to a subset of GABAergic interneurons.**  
35 **Conditional deletion of Dag1, encoding dystroglycan, in pyramidal cells caused loss of**  
36 **CCK-positive basket cell terminals in hippocampus and neocortex. PV-positive basket**  
37 **cell terminals were unaffected in mutant mice, demonstrating interneuron subtype-**  
38 **specific function of dystroglycan. Loss of dystroglycan in pyramidal cells had little**  
39 **influence on clustering of other GABAergic postsynaptic proteins and of**  
40 **glutamatergic synaptic proteins. CCK-positive terminals were not established at P21 in**  
41 **the absence of dystroglycan and were markedly reduced when dystroglycan was**  
42 **ablated in adult mice, suggesting a role for dystroglycan in both formation and**  
43 **maintenance of CCK-positive terminals. The necessity of neuronal dystroglycan for**  
44 **functional innervation by CCK-positive basket cell axon terminals was confirmed by**  
45 **reduced frequency of inhibitory events in pyramidal cells of dystroglycan-deficient**  
46 **mice and further corroborated by the inefficiency of carbachol to increase IPSC**  
47 **frequency in these cells. Finally, neurexin binding seems dispensable for dystroglycan**  
48 **function since knock-in mice expressing binding-deficient T190M dystroglycan**  
49 **displayed normal CCK-positive terminals. Taken together, we describe a novel**  
50 **function of dystroglycan in interneuron subtype-specific trans-synaptic signaling,**  
51 **revealing correlation of pre- and postsynaptic molecular diversity.**

52

### 53 **Significance statement**

54 Dystroglycan, an extracellular and transmembrane protein of the dystrophin glycoprotein  
55 complex, is at the center of molecular studies of muscular dystrophies. Although its synaptic  
56 distribution in cortical brain regions is long established, function of dystroglycan in the  
57 synapse remained obscure. Using mice that selectively lack neuronal dystroglycan, we  
58 provide evidence that a subset of GABAergic interneurons requires dystroglycan for  
59 formation and maintenance of axonal terminals on pyramidal cells. As such, dystroglycan is  
60 the first postsynaptic GABAergic protein for which an interneuron terminal-specific function  
61 could be shown. Our findings also offer a new perspective on the mechanisms that lead to  
62 intellectual disability in muscular dystrophies without associated brain malformations.

### 63 **Introduction**

64 GABAergic interneurons, which provide the main source of inhibitory drive in the adult  
65 mammalian brain, form several distinct classes according to morphological, molecular and  
66 functional criteria (Fishell and Rudy, 2011). This specialization allows interneurons to adapt  
67 to different demands of postsynaptic targets and thereby control membrane excitability in a  
68 spatially and temporally precise manner (Klausberger and Somogyi, 2008). Most interneuron  
69 classes innervate only a specific subcellular domain of target cells, for example the axon  
70 initial segment, the cell soma or dendritic regions. Synaptic transmission from different  
71 interneuron subtypes has thus fundamentally different impact on the activity of postsynaptic  
72 cells. It might be advantageous to account for this diversity of GABAergic innervation with  
73 postsynaptic specializations matching the specific properties and plasticity mechanisms of  
74 synaptic terminals they are contacted from. Indeed, the GABAergic postsynaptic density  
75 (PSD) is characterized by a large molecular heterogeneity (Tyagarajan and Fritschy, 2014).  
76 However, little is known about such subtype-specific postsynaptic GABAergic adaptations.  
77 Basket cells are GABAergic interneurons that specifically target the perisomatic region of  
78 principal neurons. In cerebral cortex and hippocampus, expression of parvalbumin (PV) or  
79 cholecystokinin (CCK) identifies basket cells as belonging to one of two non-overlapping  
80 groups (Freund and Katona, 2007). Although these two interneuron subtypes innervate the

81 same subcellular domain, they are distinguished by various traits (Bartos and Elgueta, 2012).  
82 Only CCK-positive basket cells express presynaptic cannabinoid receptors, enabling  
83 retrograde signaling of endocannabinoids to suppress GABA release. Different firing  
84 patterns, expression profiles and developmental origins further set the two subtypes apart.  
85 Therefore, it is conceivable that the two types of basket cells use different mechanisms for  
86 synapse formation and require a different set of postsynaptic proteins to exert their vastly  
87 different functions.

88 Dystroglycan (DG) is the central component of the dystrophin glycoprotein complex (DGC).  
89 The extracellular  $\alpha$ -DG and transmembrane  $\beta$ -DG, generated by proteolytic cleavage of a  
90 single gene product, bind the large cytoplasmic protein dystrophin, which in turn can interact  
91 with actin filaments.  $\alpha$ -DG, through its glycosyl side chains, can bind to extracellular matrix  
92 components. The crucial role of the DGC in muscle tissue was revealed by mutations  
93 affecting DGC components that lead to muscular dystrophies (McNally and Pytel, 2007). The  
94 DGC, albeit differing slightly in its molecular composition, is also expressed in the central  
95 nervous system by glial cells and neurons (Waite et al., 2012). Developmental brain  
96 malformations and intellectual disability, observed frequently in muscular dystrophies caused  
97 by DGC dysfunction, testify to the importance of this complex for brain function. The finding  
98 that the DGC is present in pyramidal cells as large, mostly perisomatic clusters postsynaptic  
99 to GABAergic terminals spurred interest in the synaptic function of the DGC (Lidov et al.,  
100 1990). Because reduced GABA<sub>A</sub>R immunoreactivity was found in a mouse model of  
101 Duchenne's muscular dystrophy (DMD), a function for the DGC in clustering of PSD  
102 components was posited (Knuesel et al., 1999; Vaillend et al., 2010). Despite the selective  
103 DGC subcellular distribution, biochemical interaction with presynaptic neurexins and the  
104 obligatory association of DG with GABAergic presynaptic terminals in neuronal cultures, the  
105 role of the DGC in trans-synaptic signaling was never systematically assessed (Sugita et al.,  
106 2001; Brunig et al., 2002).

107 We hypothesized that the diversity of GABAergic PSD composition is functionally related to  
108 the heterogeneity of GABAergic innervation. Due to its restricted distribution and known role

109 as a transmembrane complex, DG seemed ideally suited to address this issue. Ablation of  
110 DG specifically in pyramidal neurons allowed us to study the synaptic function of the DGC  
111 without confounding deficits in neuronal migration associated with loss of DG in other  
112 tissues. Using this approach, we demonstrate that the neuronal DGC plays an essential role  
113 in trans-synaptic signaling necessary for formation and maintenance of functional axon  
114 terminals from CCK-positive basket cells. Since the neuronal circuits depending on this  
115 signaling have been shown to be involved in major cognitive functions, our findings open new  
116 avenues in identifying the causes of intellectual disability in muscular dystrophies.

## 117 **Materials and Methods**

118 *Animals.* All mice were bred on C57BL/6 background at the Laboratory Animal Service  
119 Center (Schlieren, Zurich, Switzerland) and kept in standard housing with food and water  
120 provided *ad libitum*. Mice harboring loxP sites in exon 2 of *Dag1* were obtained from The  
121 Jackson Laboratory (Bar Harbor, ME). NEX-Cre transgenic mice were provided by Dr.  
122 Sandra Goebbels (Max-Planck-Institute of Experimental Medicine, Goettingen, Germany).  
123 *Dag1* T190M knock-in mice were provided by Dr. Kevin P. Campbell (Howard Hughes  
124 Medical Institute, Iowa City, IA). *Dag1* floxed mice were genotyped by PCR analysis using  
125 primers 5'-GGAGAGGATCAATCATGG-3' and 5'-CAACTGCTGCATCTCTAC-3'. Genotyping  
126 of NEX-Cre transgenic mice was performed as described (Goebbels et al., 2006). To obtain  
127 DG cKO and control mice, NEX-Cre<sup>tg/+</sup> / *Dag1*<sup>loxP/+</sup> mice were bred to NEX-Cre<sup>+/+</sup> /  
128 *Dag1*<sup>loxP/loxP</sup> mice. All experiments were approved by the veterinary office of the Canton of  
129 Zurich.

130 *Western blotting.* Adult DG cKO and control mice of both sexes were anaesthetized with  
131 pentobarbital (Nembutal; 50 mg/kg intraperitoneally) and sacrificed by decapitation. Cheek  
132 muscle was dissected on ice and transferred to lysis buffer (50 mM Tris (pH 7.6), 150 mM  
133 NaCl, 1% Triton X-100, Complete Mini Protease Inhibitor Cocktail [Roche, Rotkreuz,  
134 Switzerland]). Tissue was Dounce homogenized, sonicated and incubated on ice for 1h.  
135 Lysates were centrifuged at 50'000 RPM for 1h at 4 °C and supernatants were stored at -80  
136 °C. For anti- $\alpha$ -DG blots, glycosylated proteins were enriched by incubating lysates with wheat

137 germ agglutinin (WGA) agarose beads (Vector Labs, Burlingame, CA) at 4 °C overnight  
138 (ON). Proteins were eluted with 300 mM N-Acetyl-glucosamine and stored at -20 °C.  
139 Laemmli buffer was added to WGA-enriched and non-enriched lysates (for loading control)  
140 and samples were run on 8% tris-glycine polyacrylamide gels. Proteins were transferred to  
141 polyvinylidene fluoride (PVDF) membranes. Mouse anti- $\alpha$ -DG (11H6C4; Millipore; 1:1000)  
142 and rabbit anti-actin (Sigma; 1:5000) antibodies were incubated in tris-buffered saline with  
143 0.05% Tween 20 (TBST) including 5% Western Blocking Solution (Roche) ON at 4 °C.  
144 Membranes were washed 5 times in TBST. Horseradish peroxidase-coupled donkey  
145 secondary antibodies (1:20'000) were incubated for 1h at room temperature (RT) and  
146 membranes were washed again 5 times in TBST. SuperSignal West Pico Chemiluminescent  
147 Substrate (Thermo Fisher Scientific, Waltham, MA) was applied and membranes were  
148 developed on X-ray film (Fujifilm, Tokyo, Japan).

149 *Tissue preparation for immunohistochemistry.* DG cKO and control mice of both sexes at the  
150 age of 8 to 12 weeks were anaesthetized by intraperitoneal pentobarbital injection  
151 (Nembutal; 50 mg/kg) and perfused transcardially with ice-cold oxygenated artificial  
152 cerebrospinal fluid (ACSF; pH 7.4) for 2 min, as described (Notter et al., 2014). Brains were  
153 immediately dissected and fixed in 4% paraformaldehyde (PFA) for 100 min on ice. After  
154 rinsing in phosphate-buffered saline (PBS), brains were incubated in 30% sucrose (in PBS)  
155 at 4 °C ON. 50  $\mu$ m thick coronal sections were cut from frozen blocks using a sliding  
156 microtome (HM400; Microm, Walldorf, Germany) and stored at -20 °C in antifreeze solution.  
157 Tissue preparation from P21 mice followed the same protocol with the following  
158 modifications: Mice were perfused with 4% PFA (after brief perfusion with PBS to rinse  
159 blood) and brains were post-fixed for 3h.

160 *Immunohistochemistry.* After rinsing once in PBS, sections were incubated in primary  
161 antibody solution (50 mM Tris, 150 mM NaCl, 0.2% Triton X-100, 2% normal goat serum  
162 (NGS), pH 7.4) with antibodies listed in Table 1. Primary antibodies were incubated at 4 °C  
163 ON, or for 3 days if DG or dystrophin was labelled. Sections were washed 3 times for 10 min  
164 in PBS and incubated in secondary antibody solution (50 mM Tris, 150 mM NaCl, 0.05%

165 Triton X-100, 2% NGS, pH 7.4) for 30 min at RT with secondary antibodies raised in goat.  
166 Antibodies conjugated to Alexa Fluor 488 and Alexa Fluor 647 (Invitrogen, La Jolla, CA) were  
167 diluted 1:1000 whereas antibodies conjugated to Cy3 (Jackson ImmunoResearch, West  
168 Grove, PA) were diluted 1:500. Sections were washed 3 times for 10 min in PBS and  
169 mounted on gelatin-coated slides using Fluorescence Mounting Medium (Dako, Carpinteria,  
170 CA).

171 *Image analysis.* Z-stack images (3 optical sections, 0.5  $\mu\text{m}$  step size) were recorded of all  
172 specimens using confocal laser scanning microscopy (LSM 700, Carl Zeiss, Oberkochen,  
173 Germany). Images were taken using a 40x objective with a numerical aperture of 1.4 and  
174 had a pixel size of 112 x 112  $\text{nm}^2$ . To reduce variability, 3-4 sections were imaged per mouse  
175 and cluster density values were averaged from these sections. All imaging parameters were  
176 kept constant between genotypes. For cluster analysis, maximum intensity projections were  
177 created from z-stacks and analyzed using ImageJ (NIH, Bethesda, MD). Representative  
178 example images were processed with Imaris (Bitplane, Belfast, UK).

179 *Stereotactic injections.* 8 to 10 weeks old mice transgenic for loxP in exon 2 of *Dag1* were  
180 anaesthetized with isoflurane (Attane; Piramal, Mumbai, India). After mice were head-fixed  
181 on a stereotactic frame (David Kopf Instruments, Tujunga, CA), a small longitudinal incision  
182 was made under continuous administration of isoflurane to reveal the skull. Bregma was  
183 identified and the skull was perforated unilaterally using a surgical drill at the following  
184 coordinates relative to Bregma:  $x = -1.9 \text{ mm}$ ,  $y = 1.6 \text{ mm}$ . A glass pipette filled with virus  
185 solution was inserted into the brain to  $z = 1.5 \text{ mm}$ . A total of 1  $\mu\text{L}$  virus solution was injected  
186 using an automated injection pump in increments of 70 nL over 10 min. The pipette was  
187 removed and the incision sutured. Mice were injected intraperitoneally with 1 mg/kg  
188 buprenorphine (Temgesic; Essex Chemicals, Lucerne, Switzerland) and placed on a warm  
189 pad for recovery before returning to the home cage.

190 *Virus.* AAV8-CaMKIIa-mCherry-Cre (dot blot titer  $4.7 \times 10^{12}$  VG/mL) was purchased from the  
191 University of North Carolina Vector Core (Chapel Hill, NC).

192 *Acute brain slice preparation.* 5 to 6 weeks old DG cKO and control mice were briefly  
193 anaesthetized with isoflurane and decapitated. The brain was quickly removed and  
194 transferred to ice-cold solution containing 65 mM NaCl, 2.5 mM KCl, 1.25 mM NaH<sub>2</sub>PO<sub>4</sub>, 25  
195 mM NaHCO<sub>3</sub>, 7 mM MgCl<sub>2</sub>, 0.5 mM CaCl<sub>2</sub>, 25 mM glucose and 105 mM sucrose saturated  
196 with 95% O<sub>2</sub> and 5% CO<sub>2</sub>. 350 µm-thick transverse slices containing the hippocampus were  
197 cut from the tissue block with a vibratome (Microm HM 650V, Thermo Scientific, Waltham,  
198 MA) and kept in oxygenated ACSF (315 mOsm) containing 125 mM NaCl, 2.5 mM KCl, 1.25  
199 mM NaH<sub>2</sub>PO<sub>4</sub>, 25 mM NaHCO<sub>3</sub>, 1 mM MgCl<sub>2</sub>, 2 mM CaCl<sub>2</sub> and 25 mM glucose at 34 °C for  
200 25 min and then at room temperature until use.

201 *Electrophysiology and data analysis.* For recording, individual slices were transferred to a  
202 recording chamber perfused with oxygenated ACSF solution (same as above) at a flow rate  
203 of 1 to 2 mL/min. Whole-cell recordings were made from hippocampal CA1 pyramidal  
204 neurons. Cells were first selected using oblique IR illumination with a BX51 microscope (40x  
205 water-immersion objective; Olympus, Tokyo, Japan). Subsequently, neurons were  
206 anatomically identified using a fluorescent dye (Alexa 488, 10 µM) included in the  
207 intracellular solution. The dye was excited with wLS broad-band LED illumination (488 nm)  
208 and images were acquired with Retiga R1 camera using Ocular software (Qimaging, Surrey,  
209 Canada). The cells were patched with borosilicate glass pipettes (2-5 MΩ) containing: 135  
210 mM KCl, 10 mM HEPES, 10 mM sodium phosphocreatine, 4 mM Mg-ATP, 0.3 mM Na-GTP,  
211 pH 7.3 with KOH. Recordings were performed using Multiclamp 700B amplifier and data  
212 were acquired with a Digidata 1550A 16-bit board (all from Molecular Devices, Sunnyvale,  
213 CA). All experiments were performed at room temperature. Spontaneous inhibitory  
214 postsynaptic currents (sIPSC) were recorded from CA1 pyramidal cells clamped at a  
215 membrane voltage of -70 mV in the presence of 10 µM NBQX to block excitatory  
216 transmission. Recordings with unstable baseline or greater than -400 pA were rejected.  
217 Currents were filtered off-line using a Butterworth low-pass filter (2 kHz) and analyzed in 1 or  
218 2 min bins using the Mini-Analysis Program 6.0.7 (Synaptosoft, Decatur, GA). For  
219 pharmacology, baseline was analyzed 2 minutes before the application of carbachol (CCh,



220 10  $\mu$ M). To study the effect of CCh, 1-2 min bins were analyzed at least 8 minutes following  
221 the arrival of CCh into the bath. Recordings with leak increasing more than 100 pA and  
222 access resistance changing more than 30% between the beginning and the end of the  
223 recording were discarded. At least 100 events were analyzed for any condition in any  
224 experiment. Events were identified as sIPSC by setting the event detection threshold at least  
225 2-fold the baseline noise level and by checking that events had (i) rise times faster than the  
226 decay time, (ii) rise times greater than 0.5 ms and (iii) decay times greater than 1.5 ms.  
227 Events not fitting the above parameters were rejected. Event amplitudes, inter-event  
228 intervals, rise and decay times were first averaged within each experiment and regrouped by  
229 condition. The frequencies were calculated from the inter-event intervals and the resulting  
230 means were averaged between experiments. Single cell properties (access resistance,  
231 membrane capacitance, etc.) were analyzed with Clampfit 10.5 (Axon instruments, Union  
232 City, CA). Graphs were done using Igor 6.37 software (Wavemetrics, Tigard, OR) and  
233 Illustrator 15.1.0 (Adobe, San José, CA).

## 234 **Results**

### 235 **Use of NEX-Cre driver line for pyramidal cell-specific DG ablation**

236 To study the role of neuronal DGC in the brain without gross morphological alterations, it is  
237 necessary to target DG in neurons but spare glial DG. For this reason, mice harboring loxP  
238 sites in *Dag1* were crossed to the NEX-Cre driver line, which exhibits an exclusively neuronal  
239 Cre recombinase expression pattern (Goebbels et al., 2006; Satz et al., 2010). In  
240 hippocampus and neocortex, NEX promoter-mediated Cre expression is restricted to  
241 pyramidal cells, the cell type displaying most prominent DG expression in the forebrain. DG  
242 conditional knockout mice (cKO; NEX-Cre<sup>Tg/+</sup>, *Dag1*<sup>loxP/loxP</sup>) showed reduced size compared  
243 to control mice (NEX-Cre<sup>Tg/+</sup>, *Dag1*<sup>loxP/+</sup>; Figure 1A). The smaller size was reflected in  
244 reduced body and brain weight (Figure 1B and C;  $25.3 \pm 1.0$  g [mean  $\pm$  SEM] versus  $18.7 \pm$   
245  $1.0$  g,  $t_{28}=4.670$ ,  $p<0.001$  and  $473.1 \pm 5.4$  mg versus  $436.4 \pm 6.5$  mg,  $t_{28}=4.381$ ,  $p<0.001$ ,  
246 unpaired t-tests). Although cKO mice were born in Mendelian proportions, in adulthood less  
247 than the expected 25% cKO were observed due to higher lethality of cKO mice (Figure 1D).

248 To exclude a contribution of muscular dystrophy to this phenotype because of Cre leakage in  
249 muscle cells,  $\alpha$ -DG levels were examined by Western blotting of WGA-enriched muscle  
250 proteins. cKO mice showed similar levels of muscle  $\alpha$ -DG as control mice (Figure 1E). As  
251 reported before, DG cKO mice retained proper lamination of hippocampus (Figure 1F) and  
252 neocortex (Figure 1G) according to NeuN and DAPI labeling (Satz et al., 2010). Cre  
253 expression was restricted to pyramidal cells in hippocampus and neocortex and was not  
254 detected in dentate gyrus granule cells of adult mice (Figure 1F and G) (Goebbels et al.,  
255 2006).

256 Efficiency and specificity of DG ablation was examined immunohistochemically in relevant  
257 brain regions.  $\alpha$ -DG,  $\beta$ -DG and dystrophin can be detected immunohistochemically in large  
258 perisomatic clusters in CA1 pyramidal cells (Figure 2A) (Lidov et al., 1990; Knuesel et al.,  
259 1999). This characteristic immunolabeling was absent in DG cKO mice for DG and to the  
260 same extent for dystrophin, showing that dystrophin needs DG for synaptic clustering *in vivo*.  
261 In neocortex, perisomatic distribution of  $\alpha$ -DG,  $\beta$ -DG and dystrophin was replaced by diffuse  
262 unspecific staining in neuropil in DG cKO mice (Figure 2B). Astrocyte endfeet are labeled  
263 prominently by antibodies to  $\beta$ -DG and dystrophin and this labeling was preserved in DG  
264 cKO mice, as expected from neuron-specific Cre expression (asterisks in Figure 2A and B).  
265  $\alpha$ -DG immunolabeling in dentate gyrus granule cells showed the same clustered distribution  
266 in both genotypes (Figure 2C). The transient NEX promoter activity in these cells during early  
267 postnatal development might not be sufficient to achieve recombination (Goebbels et al.,  
268 2006). Alternatively, loss of DG during early development might be of little consequence in  
269 adulthood because of DG expression by granule cells that were born later. To further  
270 demonstrate specificity of NEX-induced DG ablation, striatum was selected as a control  
271 region. As expected, the characteristic sparse  $\alpha$ -DG labeling persisted in striatum of DG cKO  
272 mice (Figure 2D).

### 273 **Loss of neuronal DG results in minor alterations in GABAergic PSD protein clustering**

274 Dependence of GABAergic postsynaptic density (PSD) proteins on the DGC for synaptic  
275 clustering was suggested because of the subcellular localization of the DGC, its molecular

276 interactions and because a reduction in GABA<sub>A</sub>R clustering was observed in mice lacking  
277 full-length dystrophin (Knuesel et al., 1999; Sumita et al., 2007; Waite et al., 2012). However,  
278 requirement of DG for clustering of GABAergic postsynaptic proteins was never  
279 systematically tested *in vivo*. We hypothesized that loss of neuronal DG affects neuroligin 2  
280 (NL2) clustering, which might be important for clustering of GABA<sub>A</sub>Rs at perisomatic  
281 synapses through its interaction with gephyrin (Poulopoulos et al., 2009; Panzanelli et al.,  
282 2011). DG cKO and control mice were analyzed for changes in clustering of these markers in  
283 CA1 pyramidal layer. As previously reported (Knuesel et al., 1999; Brunig et al., 2002; Levi et  
284 al., 2002), extensive colocalization of  $\alpha$ -DG and dystrophin was observed with GABAergic  
285 markers, with a minority of DGC clusters showing no colocalization (Figure 3A and B;  
286 arrowheads and arrows, respectively). Visual examination of GABAergic markers revealed  
287 no obvious differences between genotypes (Figure 3A-C). However, quantification of cluster  
288 density and size showed a significant decrease of GABA<sub>A</sub>R  $\alpha$ 1 subunit size in cKO  
289 accompanied by an increase of GABA<sub>A</sub>R  $\alpha$ 2 subunit density (Figure 3D and F). No changes  
290 were observed in GABA<sub>A</sub>R  $\gamma$ 2 subunit and gephyrin clustering (Figure 3E and H), indicating  
291 that total synaptic GABA<sub>A</sub>R content might be unchanged whereas  $\alpha$  subunit composition is  
292 altered by loss of DG. Surprisingly, NL2 clustering was barely affected in cKO mice, showing  
293 no difference in density and only a slight but significant reduction in cluster size (Figure 3G).  
294 Neuronal DGC is also dispensable for normal colocalization of GABA<sub>A</sub>R  $\gamma$ 2 subunit with  
295 gephyrin and of  $\alpha$ 1 subunit with NL2 (Figure 3I). Furthermore, dystrophin was suggested to  
296 be important for anchoring synArfGEF at GABAergic PSDs (Fukaya et al., 2011). Although  
297 dystrophin clustering is lost in DG cKO mice, synArfGEF distribution remained almost  
298 unchanged in CA1 pyramidal layer of cKO mice (Figure 3J).

### 299 **Neuronal DG ablation leads to selective loss of markers of CCK-positive basket cell** 300 **terminals**

301 Many binding partners of  $\alpha$ -DG have been identified, among them the presynaptic neurexins  
302 (Sugita et al., 2001). Taken together with the observation that DG is always apposed to  
303 GABAergic presynaptic terminals in primary neuronal culture, a trans-synaptic function for

304 DG seemed probable (Brunig et al., 2002). We therefore probed DG cKO and control brains  
305 tissue with antibodies to presynaptic GABAergic markers. Perisomatic GABAergic terminals  
306 can be attributed to parvalbumin (PV)- or cholecystinin (CCK)-positive interneurons, which  
307 are labeled by PV / synaptotagmin 2 (Syt2) and CCK8 / VGLuT3 / cannabinoid receptor 1  
308 (CB1), respectively. We found that markers for presynaptic terminals from CCK-positive  
309 interneurons were virtually absent in CA1 pyramidal layer of DG cKO mice (Figure 4A-D, G, I  
310 and K). Still, like in control mice, CCK-positive cell somata were occasionally observed in  
311 cKO CA1 pyramidal layer, and these were often covered with VGLuT3-positive boutons  
312 (arrowheads in Figure 4A). Syt2 and PV immunolabeling were still present in typical punctate  
313 distribution in the pyramidal layer of cKO mice (Figure 4A-D, H and J), demonstrating specific  
314 requirement of DG for formation of presynaptic terminals from CCK-positive interneurons.  
315 Preferential apposition of DG to CCK-positive interneuron terminals might be expected from  
316 this finding. However, apposition of DG to VGLuT3 as well as to PV suggests no such  
317 distinction, at least at the resolution of conventional confocal laser scanning microscopy  
318 (arrowheads in C). Still, as percentage of presynaptic immunofluorescence apposed to DG,  
319 VGLuT3 showed more complete overlap with DG, indicating PV apposition to DG might be  
320 caused by mere abundance of PV immunofluorescence in the pyramidal layer (data not  
321 shown). Loss of CCK-positive interneuron terminals extended from CA3 to CA1 (Figure 4E).  
322 Surprisingly, no corresponding reduction in VGAT puncta was observed (Figure 4F).  
323 Because the DGC is prominently expressed by pyramidal cells in the neocortex, it seemed  
324 likely that CCK-positive interneuron terminals in neocortex are also compromised by loss of  
325 neuronal DG. Indeed, CCK8 and CB1 immunolabeling was strongly reduced in primary  
326 somatosensory cortex (S1) of DG cKO mice whereas PV staining was unchanged (apart  
327 from a minute difference in size; Figure 5). VGLuT3 puncta density was not decreased in  
328 neocortex of DG cKO mice, in agreement with histological studies showing VGLuT3 is  
329 present mostly in serotonergic fibers in this brain area (Figure 5B and G)(Schafer et al.,  
330 2002). As in hippocampus, reduction of CCK-positive terminals was not paralleled by a  
331 decrease of VGAT puncta (Figure 5A and E). Markers for CCK-positive terminals were

332 reduced uniformly across all cortical layers and in all regions of the neocortex which were  
333 examined (Figure 5D).

334 Satz et al. (2010) have reported blunted long-term potentiation in CA1 pyramidal cells of  
335 mice with NEX-Cre-mediated DG ablation. To exclude that loss of CCK-positive interneuron  
336 terminals represents compensatory changes to large glutamatergic alterations, glutamatergic  
337 markers were examined as a proxy for integrity of glutamatergic synapses (Figure 6).  
338 Clustering of the postsynaptic glutamatergic markers PSD-95 and bassoon did not differ  
339 significantly between genotypes (Figure 6A and B) and neither did VGLuT1 immunolabeling  
340 (Figure 6C). Furthermore, the portion of PSD-95 clusters apposed to VGLuT1 was similar in  
341 both genotypes (Figure 6D).

#### 342 **Formation and maintenance of CCK-positive basket cell terminals require neuronal DG**

343 DG expressed by pyramidal cells might have a function in synapse formation or in guidance  
344 of a subset of axons, similar to its role in the spinal cord (Wright et al., 2012). Alternatively, a  
345 function in maintenance of synapses through continuous trans-synaptic signaling is  
346 conceivable. If neuronal DG is crucial for synapse formation of CCK-positive terminals, these  
347 boutons should be reduced to the same degree as in adults at a time point right after initial  
348 synaptogenesis. Following this reasoning, we examined CCK-positive terminals of 21-day-  
349 old DG cKO and control mice in CA1 pyramidal layer. Indeed, VGLuT3 puncta were largely  
350 missing also at this stage of development whereas immunostaining of PV-positive terminals  
351 was not significantly different between genotypes (Figure 7).

352 Although this finding indicates that synapse formation of functional CCK-positive terminals  
353 depends on DG, it does not rule out a role for DG in maintaining already formed connections.  
354 In order to assess this putative function of DG in synapse maintenance, we ablated DG long  
355 after developmental synapse formation, by viral delivery of Cre to adult mice carrying one or  
356 both floxed *Dag1* alleles. AAV8-CaMKII-mCherry-Cre was stereotactically injected  
357 unilaterally into the CA1 region and mice sacrificed at 14, 28, 42 or 84 days post injection  
358 (dpi; Figure 8A and C). At 14 dpi, Cre as well as mCherry fluorescence were clearly visible  
359 (Figure 8B). Loss of  $\beta$ -DG staining at 28 dpi in homozygously floxed mice indicated efficient

360 recombination of loxP sites (Figure 8D). In heterozygously floxed mice only a moderate  
361 reduction of  $\beta$ -DG labeling was observed, suggesting one wildtype allele is sufficient to  
362 sustain the bulk of DG expression. Because dystrophin immunostaining revealed a reduction  
363 that mirrored  $\beta$ -DG, and in addition showed lower background, dystrophin was used to  
364 assess DGC loss at subsequent time points (Figure 8E-G). Examination of VGluT3-positive  
365 terminals at 28 dpi in Cre-expressing regions of CA1 pyramidal layer revealed a moderate  
366 but significant reduction of VGluT3 puncta density and size in homozygously floxed mice  
367 compared to contralateral side as well as compared to the ipsilateral side of heterozygously  
368 floxed mice (Figure 8H). VGluT3-positive terminals in heterozygous mice were not affected.  
369 Compromised VGluT3 immunolabeling was also found at later time points in homozygous  
370 mice, and the effect became more prominent with increased time after injection (Figure 8I  
371 and J). Together, these results provide strong evidence for a role of DG both in synapse  
372 formation and in retrograde trans-synaptic signaling for maintenance of CCK-positive  
373 terminals.

#### 374 **Absence of CCK-positive basket cell terminals due to DG ablation impacts pyramidal** 375 **cell inhibitory input and response to cholinergic activation**

376 If axon terminals from CCK-positive basket cells are indeed lost in DG ablated mice, this  
377 should be reflected by functional changes of pyramidal cell inhibitory input. To test this  
378 hypothesis, acute slices were prepared from adult DG cKO and control brains and used for  
379 patch-clamp electrophysiological recordings from morphologically identified CA1 pyramidal  
380 cells (Figure 9). With inhibitors of glutamatergic transmission present in the bath, occurrence  
381 of spontaneous inhibitory postsynaptic currents (sIPSCs) was probed in both genotypes. As  
382 anticipated from immunohistological changes, sIPSC frequency in DG cKO was reduced to  
383 about half of that in control slices (Figure 9;  $8.71 \pm 1.52$  Hz versus  $4.46 \pm 0.90$  Hz,  $t_{26}=2.214$ ,  
384  $p=0.036$ , unpaired t-test). Furthermore, DG cKO pyramidal cells were marked by a  
385 significantly smaller sIPSC amplitude than that of control cells ( $61.49 \pm 7.90$  pA versus  $39.18$   
386  $\pm 2.39$  pA,  $t_{26}=2.374$ ,  $p=0.025$ , unpaired t-test). No significant differences were found  
387 between genotypes in sIPSC rise and decay times (rise time  $1.73 \pm 0.09$  ms versus  $1.63 \pm$

388 0.12 ms,  $t_{26}=0.664$ ,  $p=0.512$ , unpaired t-test; decay time  $14.84 \pm 0.64$  ms versus  $14.21 \pm 0.53$   
389 ms,  $t_{26}=0.717$ ,  $p=0.480$ , unpaired t-test).

390 The differences observed in baseline sIPSCs could be due to a general reduction of  
391 inhibitory transmission instead of interneuron subtype-specific loss of terminals. In order to  
392 gain insight into the origin of reduced inhibitory transmission in DG cKO pyramidal cells, we  
393 examined the effect of the acetylcholine receptor agonist carbachol on inhibitory currents. In  
394 slices, carbachol exposure leads to an increase of perisomatic inhibitory transmission in  
395 pyramidal cells, which is mediated by direct excitation of CCK-positive interneurons (Nagode  
396 et al., 2014). Given that CB1 receptor-containing terminals are required for increased  
397 inhibitory transmission after application of carbachol, this effect should be absent in DG cKO  
398 mice, if CCK-positive basket terminals are indeed non-functional in these mice. Carbachol  
399 was bath-applied to DG cKO and control acute slices from which sIPSCs were recorded in  
400 CA1 pyramidal cells. In control slices, carbachol led to a robust increase in sIPSC frequency  
401 within minutes after application (Figure 10A-C; frequency:  $6.15 \pm 1.45$  Hz versus  $10.53 \pm$   
402  $2.47$  Hz,  $t_7=3.522$ ,  $p=0.010$ ; amplitude:  $63.36 \pm 8.84$  pA versus  $70.35 \pm 12.59$  pA,  $t_7=0.943$ ,  
403  $p=0.377$ ; paired t-tests). However, no statistically significant effect of carbachol was observed  
404 in DG cKO pyramidal cells (Figure 10D-F; frequency:  $3.45 \pm 0.75$  Hz versus  $4.47 \pm 1.56$  Hz,  
405  $t_6=0.797$ ,  $p=0.456$ ; amplitude:  $45.70 \pm 4.17$  pA versus  $53.03 \pm 5.00$  pA,  $t_6=1.239$ ,  $p=0.262$ ;  
406 paired t-tests). Together with the results from baseline recordings and immunohistochemical  
407 analysis, these findings strongly argue that functional connectivity between CCK-containing  
408 basket cells and pyramidal cells is lost in DG-ablated mice.

#### 409 **Persistence of CCK-positive terminals in DG T190M knock-in mice suggests trans-** 410 **synaptic DG function is independent of neurexin binding**

411 The intriguing finding that DG is required for formation and maintenance of CCK-positive  
412 terminals calls for an assessment of the clinical significance of this observation. In a  
413 subgroup of dystroglycanopathies, intellectual disability, although severe, is not accompanied  
414 by neuronal migration deficits (Godfrey et al., 2007). *Dag1* T190M knock-in mice are a model  
415 of one such form of dystroglycanopathy and resemble the symptoms found in patients with

416 the corresponding mutation (Dincer et al., 2003; Hara et al., 2011). Interestingly, this  
417 mutation abolishes binding of DG to neurexin, a putative presynaptic DG binding partner. We  
418 compared markers of CCK-positive terminals in CA1 pyramidal layer of homozygous *Dag1*  
419 T190M mice to wildtype mice (Figure 11). Surprisingly, both VGluT3 and CB1 puncta were  
420 indistinguishable between *Dag1* T190M and wildtype mice. Weaker and more diffuse labeling  
421 in *Dag1* T190M mice using the  $\alpha$ -DG glycosylation-specific antibody 11H6 confirmed that this  
422 mutation affects glycosylation of neuronal DG (Figure 11B). Apposition of  $\beta$ -DG to PV or  
423 VGluT3-positive terminals was not changed by T190M mutation (Figure 11E). Therefore, DG  
424 function for CCK-positive terminals is likely neurexin-independent, which suggests a novel  
425 presynaptic receptor might be involved in this trans-synaptic connection.

## 426 **Discussion**

427 Our experiments have yielded five main findings about the synaptic function of DG. Ablation  
428 of neuronal DG, which also hindered synaptic clustering of dystrophin, led only to minor  
429 changes in clustering of GABAergic PSD proteins. These alterations might reflect  
430 compensatory changes to the massive presynaptic defects found in DG-deficient mice.  
431 Importantly, DG synaptic function is interneuron subtype-specific since loss of synaptic  
432 markers was restricted to CCK-expressing basket cell terminals. Formation and maintenance  
433 of these synapses required neuronal DG, indicating that trans-synaptic signaling is important  
434 both at the time of developmental synaptogenesis and continuously during adulthood.  
435 Function of CCK-positive basket cell terminals was likely compromised along with specific  
436 marker expression, since loss of DG resulted in a reduced baseline spontaneous inhibitory  
437 activity in pyramidal cells that could not be increased by carbachol. Finally, post-  
438 phosphorylation glycosylation of DG is not necessary for CCK-positive synapse formation  
439 because *Dag1* T190M knock-in mice showed normal CCK-positive terminals, suggesting that  
440 presynaptic receptors other than neurexins might be involved in DG trans-synaptic function.



441 **Postsynaptic GABAergic alterations ascribed to DGC deficits may be secondary to**  
442 **innervation defects**

443 Ablation of DG in primary hippocampal culture has revealed that DG is not necessary for  
444 GABAergic synapse formation and for clustering of main GABAergic PSD proteins, including  
445 GABA<sub>A</sub>Rs (Levi et al., 2002). Yet, involvement of the DGC in clustering of GABAergic  
446 postsynaptic proteins was supported by several lines of evidence. Mdx mice, used as a DMD  
447 model because of their lack of full-length dystrophin, were shown to have reduced GABA<sub>A</sub>R  
448 (but not gephyrin) clustering in the hippocampus CA1 region (Knuesel et al., 1999).  
449 Overexpression of a shorter dystrophin construct *in vivo* rescued the decrease of GABA<sub>A</sub>R  
450 cluster density and size, adding to the notion that dystrophin loss directly caused GABA<sub>A</sub>R  
451 clustering defects (Vaillend et al., 2010). Neuroligin 2 (NL2) was shown to biochemically  
452 interact with dystrophin over the intracellular synaptic scaffolding molecule S-SCAM (Sumita  
453 et al., 2007). Furthermore, a functional connection between the DGC and NL2 is suggested  
454 by the observation that in GABA<sub>A</sub>R  $\alpha$ 2 subunit KO mice NL2 clustering is only compromised  
455 in dendritic but not in perisomatic areas (Panzanelli et al., 2011). The modest increase in  
456 GABA<sub>A</sub>R  $\alpha$ 2 subunit density and decrease in GABA<sub>A</sub>R  $\alpha$ 1 subunit size found in the present  
457 study does not correspond to the findings in mdx mice, in which both subunits cluster less  
458 efficiently than in wildtype mice (Knuesel et al., 1999; Vaillend et al., 2010). Rather, these  
459 alterations might reflect a subunit composition change because GABA<sub>A</sub>R  $\gamma$ 2 subunit clusters  
460 were not affected by ablation of DG (except for a minute reduction in cluster size, which  
461 might be a reflection of reduced GABA<sub>A</sub>R  $\alpha$ 1 subunit cluster size). The finding that gephyrin  
462 clustering was unchanged in DG cKO mice further supports the conclusion that overall  
463 clustering of synaptic GABA<sub>A</sub>R subunits was not influenced by neuronal DG loss. The  
464 discrepancy between our results and published data from mdx mice might be explained by  
465 different roles of dystrophin isoforms at the GABAergic PSD. Short dystrophin isoforms still  
466 present in the mdx model might, by binding to DG, cause the reduction in synaptic GABA<sub>A</sub>R  
467 clustering. It is worth noting that the  $\alpha$ 2 subunit of GABA<sub>A</sub>Rs, which is localized preferentially  
468 at CCK-positive synapses (Nyiri et al., 2001), does not require the DGC or CCK-positive

469 terminals for clustering. The DGC is thus likely involved in targeting the  $\alpha 2$  subunit to  
470 synapses apposed to CCK-positive terminals but clustering mechanisms seem to be DGC-  
471 independent. NL2 clustering was intact in DG cKO mice, apart from a slight decrease in  
472 cluster size. Therefore, the notion of the DGC as an obligatory stabilizer of postsynaptic NL2  
473 clustering by mutual interaction with S-SCAM does not hold. Similarly, a role for the DGC in  
474 clustering the dystrophin-interacting protein synArfGEF at GABAergic synapses was  
475 suggested (Fukaya et al., 2011). Not excluding a contribution of the DGC to synArfGEF  
476 function by clustering additional signaling proteins, synArfGEF does not rely on the DGC to  
477 form clustered, presumably synaptic structures.

478 In the light of the dramatic changes in GABAergic innervation due to DG loss, an indirect  
479 presynaptic contribution to reduced postsynaptic clustering in dystrophin-deficient models  
480 should be considered. This hypothesis is supported also by the finding of reduced CCK-  
481 positive basket cell markers in mdx mice, suggesting that dystrophin plays part in trans-  
482 synaptic signaling (Krasowska et al., 2014). The role of dystrophin in clustering signaling  
483 proteins at CCK-positive terminals is still unexplored, but might include retrograde signaling  
484 by nitric oxide synthase. Resolution of conventional confocal laser scanning microscopy is  
485 not sufficient to conclusively answer whether the DGC is restricted to synapses from CCK-  
486 positive basket cells. Although apposition of DG to PV- and CCK-positive terminals was  
487 found with approximately equal frequency (Figure 11E), the percentage of CCK-positive  
488 terminals apposed to DG was higher than that of PV-positive terminals (data not shown;  
489 Figure 4C and 7A). Therefore, it seems likely that the DGC localizes preferentially  
490 postsynaptic to CCK-positive terminals to regulate synapse formation and function.

491 **Basket cell type specificity of DG function implies specificity of trans-synaptic**  
492 **interaction with presynaptic binding partner**

493 The selective dependence of the CCK-containing subtype of basket cells on neuronal DG for  
494 innervating target cells is a major finding of our study and has far-reaching implications. The  
495 DGC indeed acts as a trans-synaptic complex in central synapses, suggesting that  
496 presynaptic, rather than extracellular binding partners, enable DGC function in this context.

497 Any such presynaptic adhesion molecule would have to be specifically localized at CCK-  
498 positive terminals. Interestingly, differential splicing of neuroligins in PV- and CCK-expressing  
499 basket cells was recently reported (Fuccillo et al., 2015). Transcripts lacking neuroligin1 $\alpha$   
500 alternative splice inserts 2 and 4, which prevent  $\alpha$ -DG binding to LSM domains 2 and 6,  
501 respectively, were only found in CCK-positive basket cells (Sugita et al., 2001; Reissner et  
502 al., 2014; Fuccillo et al., 2015). This neuroligin isoform-specificity of basket cell subtypes  
503 would provide a mechanism for selective dependence of CCK-positive basket terminals on  
504 DG. However, we found terminals from CCK-positive basket cells to be intact in *Dag1* T190M  
505 knock-in mice. DG containing the T190M mutation was found to lose neuroligin binding  
506 capacity (Hara et al., 2011). This finding thus suggests that a novel presynaptic DG binding  
507 partner might be specifically localized at CCK-positive terminals. But because the diversity of  
508 neuroligin isoforms was not considered in DG T190M binding assays, the possibility of a  
509 specific neuroligin-DG trans-synaptic complex at CCK-positive terminals remains.

510 **Continuous trans-synaptic signaling required for maintenance of CCK-positive**  
511 **terminals might reflect novel plasticity mechanism**

512 Stopping trans-synaptic signaling mediated by the DGC by ablating DG in adulthood led to a  
513 decrease of CCK-positive terminals within weeks. This unexpected result implies that DG  
514 function goes beyond a potential role in validating newly formed synapses from CCK-positive  
515 basket cells. In addition to clustering signaling molecules at these synapses, our findings  
516 open the possibility that the DGC, by forming a trans-synaptic complex, is a direct target to  
517 regulate abundance of CCK-positive terminals.  $\beta$ -DG is a substrate of MMP-9 in a neuronal  
518 activity-dependent manner (Yamada et al., 2001; Kaczmarek et al., 2002; Michaluk et al.,  
519 2007). Cleavage of DG might therefore represent a physiological interneuron subtype-  
520 specific plasticity mechanism. In striking agreement with this hypothesis, CCK-positive  
521 terminals are selectively lost in a model of temporal lobe epilepsy (Wyeth et al., 2010).

522 **Decreased inhibitory input to pyramidal cells in DG-ablated cells confirms functional**  
523 **significance of DG signaling for CCK-positive terminals**

524 The possibility that loss of CCK-specific markers in DG cKO mice is only due to inability of  
525 terminals to differentiate was ruled out by the finding that DG-ablated pyramidal cells receive  
526 reduced inhibitory drive. Along with sIPSC frequency, amplitude was markedly reduced,  
527 possibly reflecting mistargeting of GABA<sub>A</sub>Rs in the absence of the DGC. Genesis of  
528 carbachol-induced increase of inhibitory currents is not fully understood but involves Gad2-  
529 positive rather than PV-positive interneurons in the CA1 region (Nagode et al., 2014). Since  
530 the group of Gad2-expressing interneurons includes CCK-positive basket cells and  
531 carbachol-induced currents are sensitive to depolarization-induced suppression of inhibition,  
532 our results add to the notion that CCK-positive basket cells play a crucial role in carbachol-  
533 induced activity. Activity patterns elicited by carbachol correlate with behaviorally relevant  
534 theta oscillations. Mechanisms of theta oscillation generation should thus be considered in  
535 future investigations of the etiology of intellectual disability associated with muscular  
536 dystrophies.

537 **Conclusions**

538 Our investigation of the role of neuronal DG in GABAergic synapses has revealed a  
539 surprising interneuron type-specific function of DG in trans-synaptic signaling. It has shown  
540 that GABAergic postsynaptic diversity is functionally related to interneuron subtype  
541 heterogeneity and supports the emerging notion of a cell type-specific molecular code of  
542 synapse formation. Future studies will have to further characterize signaling and plasticity  
543 enabled by the DGC and delineate its behavioral consequences. Taking the interneuron-  
544 specific role of DG into consideration will help elucidate the mechanisms underlying  
545 intellectual disability observed in muscular dystrophies without developmental brain  
546 malformations.

547 **References**

548 Bartos M, Elgueta C (2012) Functional characteristics of parvalbumin- and cholecystinin-  
549 expressing basket cells. J Physiol 590:669-681.

550 Brunig I, Suter A, Knuesel I, Luscher B, Fritschy JM (2002) GABAergic terminals are required  
551 for postsynaptic clustering of dystrophin but not of GABA(A) receptors and gephyrin. *J*  
552 *Neurosci* 22:4805-4813.

553 Dincer P, Balci B, Yuva Y, Talim B, Brockington M, Dincel D, Torelli S, Brown S, Kale G,  
554 Haliloglu G, Gerceker FO, Atalay RC, Yakicier C, Longman C, Muntoni F, Topaloglu H  
555 (2003) A novel form of recessive limb girdle muscular dystrophy with mental retardation and  
556 abnormal expression of alpha-dystroglycan. *Neuromuscul Disord* 13:771-778.

557 Fishell G, Rudy B (2011) Mechanisms of inhibition within the telencephalon: "where the wild  
558 things are". *Annu Rev Neurosci* 34:535-567.

559 Freund TF, Katona I (2007) Perisomatic inhibition. *Neuron* 56:33-42.

560 Fritschy JM, Mohler H (1995) GABAA-receptor heterogeneity in the adult rat brain:  
561 differential regional and cellular distribution of seven major subunits. *J Comp Neurol*  
562 359:154-194.

563 Fuccillo MV, Foldy C, Gokce O, Rothwell PE, Sun GL, Malenka RC, Sudhof TC (2015)  
564 Single-Cell mRNA Profiling Reveals Cell-Type-Specific Expression of Neurexin Isoforms.  
565 *Neuron* 87:326-340.

566 Fukaya M, Kamata A, Hara Y, Tamaki H, Katsumata O, Ito N, Takeda S, Hata Y, Suzuki T,  
567 Watanabe M, Harvey RJ, Sakagami H (2011) SynArfGEF is a guanine nucleotide exchange  
568 factor for Arf6 and localizes preferentially at post-synaptic specializations of inhibitory  
569 synapses. *J Neurochem* 116:1122-1137.

570 Godfrey C et al. (2007) Refining genotype phenotype correlations in muscular dystrophies  
571 with defective glycosylation of dystroglycan. *Brain* 130:2725-2735.

572 Goebbels S, Bormuth I, Bode U, Hermanson O, Schwab MH, Nave KA (2006) Genetic  
573 targeting of principal neurons in neocortex and hippocampus of NEX-Cre mice. *Genesis*  
574 44:611-621.

575 Hara Y, Balci-Hayta B, Yoshida-Moriguchi T, Kanagawa M, Beltran-Valero de Bernabe D,  
576 Gundesli H, Willer T, Satz JS, Crawford RW, Burden SJ, Kunz S, Oldstone MB, Accardi A,

577 Talim B, Muntoni F, Topaloglu H, Dincer P, Campbell KP (2011) A dystroglycan mutation  
578 associated with limb-girdle muscular dystrophy. *N Engl J Med* 364:939-946.

579 Kaczmarek L, Lapinska-Dzwonek J, Szymczak S (2002) Matrix metalloproteinases in the  
580 adult brain physiology: a link between c-Fos, AP-1 and remodeling of neuronal connections?  
581 *Embo J* 21:6643-6648.

582 Klausberger T, Somogyi P (2008) Neuronal diversity and temporal dynamics: the unity of  
583 hippocampal circuit operations. *Science* 321:53-57.

584 Knuesel I, Mastrocola M, Zuellig RA, Bornhauser B, Schaub MC, Fritschy JM (1999) Short  
585 communication: altered synaptic clustering of GABAA receptors in mice lacking dystrophin  
586 (mdx mice). *Eur J Neurosci* 11:4457-4462.

587 Krasowska E, Zablocki K, Gorecki DC, Swinny JD (2014) Aberrant location of inhibitory  
588 synaptic marker proteins in the hippocampus of dystrophin-deficient mice: implications for  
589 cognitive impairment in duchenne muscular dystrophy. *PLoS One* 9:e108364.

590 Levi S, Grady RM, Henry MD, Campbell KP, Sanes JR, Craig AM (2002) Dystroglycan is  
591 selectively associated with inhibitory GABAergic synapses but is dispensable for their  
592 differentiation. *J Neurosci* 22:4274-4285.

593 Lidov HG, Byers TJ, Watkins SC, Kunkel LM (1990) Localization of dystrophin to  
594 postsynaptic regions of central nervous system cortical neurons. *Nature* 348:725-728.

595 McNally EM, Pytel P (2007) Muscle diseases: the muscular dystrophies. *Annu Rev Pathol*  
596 2:87-109.

597 Michaluk P, Kolodziej L, Mioduszevska B, Wilczynski GM, Dzwonek J, Jaworski J, Gorecki  
598 DC, Ottersen OP, Kaczmarek L (2007) Beta-dystroglycan as a target for MMP-9, in response  
599 to enhanced neuronal activity. *J Biol Chem* 282:16036-16041.

600 Nagode DA, Tang AH, Yang K, Alger BE (2014) Optogenetic identification of an intrinsic  
601 cholinergically driven inhibitory oscillator sensitive to cannabinoids and opioids in  
602 hippocampal CA1. *J Physiol* 592:103-123.

603 Notter T, Panzanelli P, Pfister S, Mircsof D, Fritschy JM (2014) A protocol for concurrent  
604 high-quality immunohistochemical and biochemical analyses in adult mouse central nervous  
605 system. *Eur J Neurosci* 39:165-175.

606 Nyiri G, Freund TF, Somogyi P (2001) Input-dependent synaptic targeting of alpha(2)-  
607 subunit-containing GABA(A) receptors in synapses of hippocampal pyramidal cells of the rat.  
608 *Eur J Neurosci* 13:428-442.

609 Panzanelli P, Gunn BG, Schlatter MC, Benke D, Tyagarajan SK, Scheiffele P, Belelli D,  
610 Lambert JJ, Rudolph U, Fritschy JM (2011) Distinct mechanisms regulate GABAA receptor  
611 and gephyrin clustering at perisomatic and axo-axonic synapses on CA1 pyramidal cells. *J*  
612 *Physiol* 589:4959-4980.

613 Pouloupoulos A, Aramuni G, Meyer G, Soykan T, Hoon M, Papadopoulos T, Zhang M,  
614 Paarmann I, Fuchs C, Harvey K, Jedlicka P, Schwarzacher SW, Betz H, Harvey RJ, Brose N,  
615 Zhang W, Varoqueaux F (2009) Neuroligin 2 drives postsynaptic assembly at perisomatic  
616 inhibitory synapses through gephyrin and collybistin. *Neuron* 63:628-642.

617 Reissner C, Stahn J, Breuer D, Klose M, Pohlentz G, Mormann M, Missler M (2014)  
618 Dystroglycan binding to alpha-neurexin competes with neurexophilin-1 and neuroligin in the  
619 brain. *J Biol Chem* 289:27585-27603.

620 Satz JS, Ostendorf AP, Hou S, Turner A, Kusano H, Lee JC, Turk R, Nguyen H, Ross-Barta  
621 SE, Westra S, Hoshi T, Moore SA, Campbell KP (2010) Distinct functions of glial and  
622 neuronal dystroglycan in the developing and adult mouse brain. *J Neurosci* 30:14560-14572.

623 Schafer MK, Varoqui H, Defamie N, Weihe E, Erickson JD (2002) Molecular cloning and  
624 functional identification of mouse vesicular glutamate transporter 3 and its expression in  
625 subsets of novel excitatory neurons. *J Biol Chem* 277:50734-50748.

626 Sugita S, Saito F, Tang J, Satz J, Campbell K, Sudhof TC (2001) A stoichiometric complex of  
627 neurexins and dystroglycan in brain. *J Cell Biol* 154:435-445.

628 Sumita K, Sato Y, Iida J, Kawata A, Hamano M, Hirabayashi S, Ohno K, Peles E, Hata Y  
629 (2007) Synaptic scaffolding molecule (S-SCAM) membrane-associated guanylate kinase with

630 inverted organization (MAGI)-2 is associated with cell adhesion molecules at inhibitory  
631 synapses in rat hippocampal neurons. *J Neurochem* 100:154-166.

632 Tyagarajan SK, Fritschy JM (2014) Gephyrin: a master regulator of neuronal function? *Nat*  
633 *Rev Neurosci* 15:141-156.

634 Vaillend C, Perronnet C, Ros C, Gruszczynski C, Goyenvalle A, Laroche S, Danos O, Garcia  
635 L, Peltekian E (2010) Rescue of a dystrophin-like protein by exon skipping in vivo restores  
636 GABAA-receptor clustering in the hippocampus of the mdx mouse. *Mol Ther* 18:1683-1688.

637 Waite A, Brown SC, Blake DJ (2012) The dystrophin-glycoprotein complex in brain  
638 development and disease. *Trends Neurosci* 35:487-496.

639 Wright KM, Lyon KA, Leung H, Leahy DJ, Ma L, Ginty DD (2012) Dystroglycan organizes  
640 axon guidance cue localization and axonal pathfinding. *Neuron* 76:931-944.

641 Wyeth MS, Zhang N, Mody I, Houser CR (2010) Selective reduction of cholecystokinin-  
642 positive basket cell innervation in a model of temporal lobe epilepsy. *J Neurosci* 30:8993-  
643 9006.

644 Yamada H, Saito F, Fukuta-Ohi H, Zhong D, Hase A, Arai K, Okuyama A, Maekawa R,  
645 Shimizu T, Matsumura K (2001) Processing of beta-dystroglycan by matrix metalloproteinase  
646 disrupts the link between the extracellular matrix and cell membrane via the dystroglycan  
647 complex. *Hum Mol Genet* 10:1563-1569.

648

## 649 **Legends**

650 Figure 1. Characterization of NEX-Cre / *Dag1* conditional KO mice. A, Representative  
651 examples of NEX-Cre<sup>Tg/+</sup> / *Dag1*<sup>loxP/+</sup> (control) and NEX-Cre<sup>Tg/+</sup> / *Dag1*<sup>loxP/loxP</sup> (cKO) mice (4  
652 months of age, siblings, both female). B, cKO mice exhibit reduced body weight compared to  
653 sibling control mice. C, Wet brain weight was lower in cKO mice than in controls. D, cKO  
654 mice exhibited a higher mortality rate than control mice, resulting in a frequency of cKO mice  
655 lower than the expected 25% at the age of 10 weeks. E, Similar levels of  $\alpha$ -DG isolated from  
656 cheek muscle were found for cKO and control mice. F, Cre expression was restricted to  
657 pyramidal cells in the hippocampus of cKO and control mice. In adult mice, dentate gyrus



658 granule cells were not immunoreactive for Cre recombinase. NeuN and DAPI labeling show  
659 intact neuronal migration when NEX-Cre is used as driver line to ablate *Dag1*. G, In primary  
660 somatosensory cortex Cre expression was also restricted to pyramidal cells. No migratory  
661 deficits were found in the neocortex in cKO mice. \*\*\* $p < 0.001$ .

662 Figure 2. NEX-Cre-mediated ablation of dystroglycan leads to specific loss of dystrophin  
663 glycoprotein complex in pyramidal cells. A, Characteristic staining of  $\alpha$ - and  $\beta$ -DG and  
664 dystrophin around CA1 pyramidal layer is lost in cKO mice. Labeling of  $\beta$ -DG and dystrophin  
665 in astrocyte end-feet is retained in cKO mice (asterisks). B, In primary somatosensory cortex  
666 layer 2/3, clustered labeling of DGC components around pyramidal cells is replaced by  
667 diffuse staining in the neuropil. Astrocyte end-feet labeling of  $\beta$ -DG and dystrophin is retained  
668 in cKO mice (asterisks). C,  $\alpha$ -DG immunofluorescence in dentate gyrus is unaffected by  
669 NEX-Cre-mediated ablation of DG. D,  $\alpha$ -DG expression in striatum is unaffected in cKO  
670 mice, confirming specificity of NEX-Cre expression to pyramidal cells. SR, stratum radiatum;  
671 SP, stratum pyramidale; ML, molecular layer; GCL, granule cell layer.

672 Figure 3. Loss of neuronal dystroglycan does not prohibit formation of GABAergic PSD but  
673 leads to minor changes in GABA<sub>A</sub>R subunit clustering. A-C, Triple immunofluorescence  
674 labeling of GABAergic postsynaptic markers in pyramidal layer of hippocampus CA1 area.  
675 The DGC is largely colocalized with  $\alpha 2$  subunit and VGAT (A; arrowheads) but also with  $\alpha 1$   
676 subunit and NL2 (B; arrowheads). A minority of DGC clusters is not associated with  
677 GABAergic markers (A and B; arrows). D-H, Quantification of postsynaptic GABAergic  
678 markers in CA1 pyramidal cell layer. Cluster density and size are shown for GABA<sub>A</sub>R  $\alpha 1$  (D),  
679  $\alpha 2$  (F) and  $\gamma 2$  (H) subunits and for gephyrin (E) and NL2 (G). A decrease of  $\alpha 1$  subunit  
680 cluster size was accompanied by an increased  $\alpha 2$  subunit cluster density. I, Colocalization of  
681 postsynaptic GABAergic markers was analyzed in cKO and control mice. Data represent the  
682 number of colocalized clusters as percentage of first mentioned marker. No significant  
683 differences in colocalization were found between genotypes. J, Clustering of synArfGEF was  
684 analyzed in CA1 pyramidal layer of DG cKO and control mice. Data points represent  
685 individual mice. \*\* $p < 0.01$ , \*\*\* $p < 0.001$  (see Table 2 for statistical tests).

686 Figure 4. Neuronal dystroglycan ablation leads to specific loss of terminals from CCK-  
687 positive basket cells on hippocampal pyramidal cells. A-D, Triple immunofluorescence  
688 labeling of presynaptic GABAergic markers in hippocampus CA1 area. A, In pyramidal layer,  
689 markers labeling CCK-positive basket cell terminals (CCK8, VGlut3) are missing around  
690 pyramidal cell bodies, but are still present on CCK-positive cell somata occasionally  
691 observed near the pyramidal layer (arrows). These VGlut3-positive boutons on CCK-positive  
692 somata were often immunopositive for synaptotagmin 2. In the pyramidal layer,  
693 immunostaining for synaptotagmin 2 remained in cKO mice. B1 and B2 show separated  
694 channels of insets in A. C, PV immunolabeling in CA1 pyramidal layer of DG cKO mice is  
695 indistinguishable from control. In CA1 pyramidal layer of control mice, the majority of  $\alpha$ -DG  
696 clusters is either apposed to VGlut3 (arrow 1) or PV (arrow 2), but some clusters are not  
697 apposed to either marker (arrow 3). A minority of  $\alpha$ -DG clusters showed apposition to both  
698 VGlut3 and PV (arrow 4). D, Along with CCK8 and VGlut3, CB1 staining is strongly reduced  
699 in CA1 pyramidal layer of DG cKO mice. E, Loss of CB1 immunofluorescence in DG cKO  
700 mice was observed from CA1 to CA3. F-K, Quantification of presynaptic GABAergic markers  
701 in CA1 pyramidal layer. No changes were found for VGAT (F) and PV-positive basket cell  
702 markers (H, J) between genotypes but cluster density and size of markers of CCK-positive  
703 basket cell terminals (G, I, K) were strongly reduced in DG cKO mice. Data points represent  
704 individual mice. \*\*\* $p < 0.001$  (see Table 2 for statistical tests). SR, stratum radiatum; SP,  
705 stratum pyramidale.

706 Figure 5. Neuronal dystroglycan ablation leads to specific loss of terminals from CCK-  
707 positive basket cells on pyramidal cells in neocortex. A-C, Triple immunofluorescence  
708 labeling of GABAergic markers in layer 2/3 of primary somatosensory cortex (S1) of DG cKO  
709 and control mice. A, As in hippocampus, the majority of DG clusters is colocalized with pre-  
710 and postsynaptic GABAergic markers in neocortex. B, Neocortical PV and VGlut3  
711 immunolabeling is not affected by loss of neuronal DG. C, CCK8 and CB1  
712 immunofluorescence is strongly reduced in neocortex of DG cKO mice. Immunolabeling of  
713 synArfGEF showed clustered distribution and did not differ between genotypes. D, Overview

714 of S1 of DG cKO and control mice. Typical punctate CB1 immunofluorescence was lost  
715 across all layers of the cortex in DG cKO mice. E-I, Quantification of presynaptic GABAergic  
716 markers in S1 layer 2/3. VGAT and PV, and in contrast to hippocampus, also VGLuT3 were  
717 not reduced in density and size in mice lacking neuronal DG (E, F, G). However, CB1 and  
718 CCK8 showed a similar reduction as in hippocampus in DG cKO mice compared to control  
719 mice (H and I). Data points represent individual mice. \*\* $p < 0.01$ , \*\*\* $p < 0.001$  (see Table 2 for  
720 statistical tests).

721 Figure 6. Neuronal dystroglycan is not necessary for clustering of glutamatergic synaptic  
722 proteins. A and B, To assess integrity of glutamatergic postsynaptic structures, antibodies to  
723 PSD-95 and bassoon were used and immunofluorescence quantified in stratum pyramidale  
724 and stratum radiatum. Cluster density and size was analyzed in stratum pyramidale and  
725 fluorescence intensity in stratum radiatum. All parameters analyzed did not differ between  
726 genotypes. C, VGLuT1 was used as a marker of glutamatergic presynaptic terminals and  
727 puncta density and size in stratum pyramidale was quantified. No changes in VGLuT1 puncta  
728 density and size were found between genotypes. D, PSD-95 apposition to VGLuT1 was  
729 examined in stratum pyramidale and represented as percent PSD-95 clusters apposed to  
730 VGLuT1 puncta. The apposition of PSD-95 to VGLuT1 did not differ between genotypes. Data  
731 points represent individual mice. \* $p < 0.05$ , \*\*\* $p < 0.001$  (see Table 2 for statistical tests).

732 Figure 7. CCK-positive terminals are not established in the absence of neuronal  
733 dystroglycan. A, Triple immunofluorescence labeling of DG cKO and control CA1 pyramidal  
734 layer at postnatal day 21. B and C, Quantification of puncta density and size reveals loss of  
735 VGLuT3 puncta in DG cKO tissue to the same degree as in adult mice (B) but unchanged PV  
736 immunolabeling (C). Data points represent individual mice. \*\*\* $p < 0.001$  (see Table 2 for  
737 statistical tests).

738 Figure 8. Maintenance of CCK-positive basket terminals requires dystroglycan. A, Overview  
739 of experimental design. Virus was stereotactically injected unilaterally into CA1 region in  
740 adult mice heterozygous or homozygous for loxP sites flanking *Dag1* gene. B, After 14 dpi,  
741 Cre recombinase immunolabeling as well as mCherry fluorescence was clearly visible in

742 pyramidal cell somata. C, Example of injection site at 28 dpi. Cre expression was mostly  
743 restricted to CA1 pyramidal cell layer. VGLuT3 and dystrophin or DG immunofluorescence  
744 was analyzed in the same sections. D, In mice containing homozygously floxed *Dag1*,  $\beta$ -DG  
745 immunostaining was markedly reduced in CA1 pyramidal layer at 28 dpi. Heterozygous mice  
746 showed a moderate reduction in  $\beta$ -DG immunofluorescence. E-G, As observed for  $\beta$ -DG, Cre  
747 expression lead to loss of dystrophin in homozygously floxed mice whereas only a slight  
748 decrease was observed in heterozygous mice. Reduction of dystrophin labeling was similar at  
749 28 dpi (E), 42 dpi (F) and 84 dpi (G). H-J, Representative example images and  
750 quantifications of VGLuT3 immunostaining in CA1 pyramidal layer at 28 dpi (H), 42 dpi (I) and  
751 84 dpi (J). Ipsilateral VGLuT3 size and density in homozygously floxed mice was significantly  
752 reduced compared to both contralateral side and ipsilateral side of heterozygously floxed  
753 mice. With increased time after injection this reduction of VGLuT3 puncta became more  
754 prominent. Data points represent individual mice. \* $p < 0.05$ , \*\* $p < 0.01$ , \*\*\* $p < 0.001$  (see Table 2  
755 for statistical tests).

756 Figure 9. Frequency and amplitude of sIPSCs are reduced in dystroglycan cKO pyramidal  
757 cells. A, Image showing the position of the recording pipette in the hippocampal CA1 region  
758 (left, 4x), and an example image of a typical CA1 pyramidal cell identified using LED  
759 illumination (Alexa Fluor 488, right, 40x). B, Representative example traces of whole-cell  
760 sIPSC recordings from control mice (left trace) and DG cKO mice (right trace). Average  
761 sIPSCs are shown above the traces. C, Cumulative frequency plot of inter-event intervals of  
762 sIPSCs from control (blue line) and DG cKO cell (red line) from the traces in B (left panel)  
763 and cumulative frequency plot of sIPSC amplitudes from the same cells (right panel). D,  
764 Comparison of average sIPSC frequency and amplitude between control and DG cKO slices.  
765 DG cKO mice exhibit significantly lower sIPSC frequency and amplitude than control mice.  
766 Data points represent individual cells. \* $p < 0.05$ .

767 Figure 10. Dystroglycan is necessary for carbachol-induced increase of inhibitory currents in  
768 pyramidal cells. A, Representative example traces of sIPSC recordings before (baseline, left  
769 trace) and after the application of carbachol (CCh, right trace) in control mice. Average

770 sIPSCs are shown above the traces. B, Cumulative frequency plots of inter-event intervals  
771 (IEI) and amplitudes of sIPSCs from traces in A. C, Comparison of average sIPSC frequency  
772 and amplitude before and after application of CCh in control slices. Application of CCh  
773 resulted in typical increase of IPSC frequency in control pyramidal cells but amplitude was  
774 not affected by CCh. D, Representative example traces of sIPSC recordings before  
775 (baseline, left trace) and after the application of CCh (right trace) in DG cKO mice. Average  
776 sIPSCs are shown above the traces. E, Cumulative frequency plots of inter-event intervals  
777 (IEI) and amplitudes of sIPSCs from traces in D. F, Comparison of average sIPSC frequency  
778 and amplitude before and after application of CCh in DG cKO slices. In contrast to control  
779 slices, application of CCh did not lead to a significant increase of sIPSC frequency in DG  
780 cKO pyramidal cells. Data points represent individual cells. \*\* $p < 0.01$ .

781 Figure 11. Neurexin- and laminin-binding of  $\alpha$ -dystroglycan is not essential for formation of  
782 CCK-positive basket terminals on pyramidal cells. A and B, Triple immunofluorescence  
783 labeling of GABAergic markers in CA1 pyramidal layer of *Dag1* T190M and wildtype mice. A,  
784 Antibody to  $\beta$ -DG revealed typical clustered distribution in *Dag1* T190M mice. VGlut3 and  
785 PV immunofluorescence was indistinguishable between genotypes. B, Intensity of DG  
786 clusters was markedly reduced and background staining increased using the  $\alpha$ -DG  
787 glycosylation-specific antibody 11H6, confirming glycosylation deficits of synaptic DG in  
788 T190M mice. CB1 and GABA<sub>A</sub>R  $\gamma$ 2 subunit immunofluorescence was indistinguishable  
789 between genotypes. C and D, Quantification of density and size of VGlut3 (C) and CB1 (D)  
790 puncta in CA1 pyramidal layer of *Dag1* T190M and wildtype mice. Density and size of puncta  
791 did not differ significantly between genotypes. E, Quantification of  $\beta$ -DG apposition to PV  
792 and/or VGlut3 in CA1 pyramidal layer. Data represent number of  $\beta$ -DG clusters apposed to  
793 PV or VGlut3 or both (triple colocalized) as percentage of total  $\beta$ -DG clusters. Apposition of  
794  $\beta$ -DG to presynaptic markers did not differ significantly between genotypes. Data points  
795 represent individual mice. See Table 2 for statistical tests.

796 **Illustrations and Tables**797 **Table 1. Antibodies used for immunohistochemical stainings**

Target	Host species	Dilution	Cat. no.	Company / origin
$\alpha$ -Dystroglycan (VIA4-1)	Mouse	1:100	05-298	EMD Millipore
$\alpha$ -Dystroglycan (11H6C4)	Mouse	1:100	05-593	EMD Millipore
$\beta$ -Dystroglycan	Mouse	1:100	ab49515	Abcam
Bassoon	Mouse	1:2000	VAM-PS003	StressGen
Cannabinoid receptor 1	Rabbit	1:3000	258 003	Synaptic Systems
Cholecystokinin 8	Mouse	1:1000	ab37274	Abcam
Cre recombinase	Rabbit	1:1000	PRB-106C	Covance
Dystrophin (C-terminal)	Mouse	1:100	BT39-9050-05	Biotrend
GABA <sub>A</sub> R $\alpha$ 1 subunit	Guinea pig	1:20'000	-	(Fritschy and Mohler, 1995)
GABA <sub>A</sub> R $\alpha$ 2 subunit	Guinea pig	1:6000	-	(Fritschy and Mohler, 1995)
GABA <sub>A</sub> R $\gamma$ 2 subunit	Guinea pig	1:10'000	-	(Fritschy and Mohler, 1995)
GAD65/67	Rabbit	1:2000	GC 3008	Biomol
Gephyrin	Mouse	1:1000	147 021	Synaptic Systems
NeuN	Mouse	1:1000	MAB377	Chemicon
Neurologin 2	Rabbit	1:10'000	-	Gift from Dr. Peter Scheiffele
Parvalbumin	Rabbit	1:1000	24428	ImmunoStar
PSD-95	Mouse	1:1000	MA1-045	ABR
Synaptotagmin 2	Rabbit	1:1000	105 123	Synaptic Systems
synArfGEF	Guinea pig	1:3000	-	Gift from Dr. Hiroyuki Sakagami (Fukaya et al., 2011)
VGAT	Rabbit	1:3000	131 003	Synaptic Systems
VGluT1	Guinea pig	1:1000	135 304	Synaptic Systems
VGluT3	Guinea pig	1:4000	AB5421	Merck Millipore

798

799 Table 1. Antibodies used for immunohistochemical stainings. If not otherwise stated,  
800 antibody VIA4-1 was used to label  $\alpha$ -dystroglycan. For secondary antibodies see Materials  
801 and Methods.

802

803 **Table 2. Results of statistical tests performed for immunohistochemical stainings**

Epitope	Conditions	Unpaired t-test	
		(density)	Kolmogorov-Smirnov test (size)
GABA <sub>A</sub> R α1 subunit	DG cKO / adult / CA1	t <sub>6</sub> =0.920, p=0.393	n=33385, D=12.662, p<0.001
GABA <sub>A</sub> R α2 subunit	DG cKO / adult / CA1	t <sub>15</sub> =3.816, p=0.002	n=18495, D=3.484, p<0.001
GABA <sub>A</sub> R γ2 subunit	DG cKO / adult / CA1	t <sub>7</sub> =1.607, p=0.152	n=31807, D=3.692, p<0.001
Gephyrin	DG cKO / adult / CA1	t <sub>7</sub> =1.252, p=0.251	n=39289, D=0.720, p=0.677
Neuroigin 2	DG cKO / adult / CA1	t <sub>6</sub> =0.979, p=0.366	n=32217, D=5.476, p<0.001
synArfGEF	DG cKO / adult / CA1	t <sub>6</sub> =1.093, p=0.316	n=22737, D=3.850, p<0.001
VGAT	DG cKO / adult / CA1	t <sub>15</sub> =0.646, p=0.528	n=20569, D=0.528, p=0.943
	DG cKO / adult / neocortex	t <sub>9</sub> =1.309, p=0.223	n=24713, D=1.107, p=0.172
Parvalbumin	DG cKO / adult / CA1	t <sub>7</sub> =0.198, p=0.849	n=24929, D=1.068, p=0.204
	DG cKO / adult / neocortex	t <sub>9</sub> =0.454, p=0.661	n=20534, D=4.845, p<0.001
	DG cKO / P21 / CA1	t <sub>8</sub> =0.869, p=0.410	n=8010, D=1.037, p=0.233
Cannabinoid receptor 1	DG cKO / adult / CA1	t <sub>6</sub> =16.869, p<0.001	n=4654, D=4.325, p<0.001
	DG cKO / adult / neocortex	t <sub>11</sub> =7.117, p<0.001	n=8067, D=6.960, p<0.001
	T190M / adult / CA1	t <sub>8</sub> =0.681, p=0.515	n=9152, D=0.881, p=0.420
Synaptotagmin 2	DG cKO / adult / CA1	t <sub>9</sub> =1.456, p=0.179	n=3397, D=1.977, p=0.001
Cholecystokinin 8	DG cKO / adult / CA1	t <sub>17</sub> =6.292, p<0.001	n=5111, D=4.133, p<0.001
	DG cKO / adult / neocortex	t <sub>6</sub> =4.475, p=0.004	n=1387, D=1.874, p=0.002
PSD-95	DG cKO / adult / CA1 / SP	t <sub>6</sub> =1.106, p=0.311	n=16281, D=1.554, p=0.016
	DG cKO / adult / CA1 / SR	t <sub>6</sub> =0.243, p=0.817	-
Bassoon	DG cKO / adult / CA1 / SP	t <sub>10</sub> =0.767, p=0.461	n=32489, D=2.275, p<0.001
	DG cKO / adult / CA1 / SR	t <sub>10</sub> =0.871, p=0.404	-
VGluT1	DG cKO / adult / CA1	t <sub>6</sub> =0.094, p=0.928	n=12776, D=0.492, p=0.969
VGluT3	DG cKO / adult / CA1	t <sub>21</sub> =13.213, p<0.001	n=5975, D=8.273, p<0.001
	DG cKO / adult / neocortex	t <sub>9</sub> =0.456, p=0.659	n=6523, D=2.054, p<0.001
	DG cKO / P21 / CA1	t <sub>8</sub> =13.437, p<0.001	n=1830, D=8.270, p<0.001
	T190M / adult / CA1	t <sub>8</sub> =0.494, p=0.634	n=4763, D=0.702, p=0.708
<b>t-test (unpaired between genotypes, paired between</b>			
		<b>Kruskal-</b>	<b>Dunn's multiple</b>

<b>Conditions</b>	<b>hemispheres; density)</b>	<b>Wallis test (size)</b>	<b>comparison test (size)</b>
28dpi / loxP/+	t <sub>3</sub> =0.520, p=0.639	n=13610	y=283.498, p<0.05
28dpi / loxP/loxP	t <sub>4</sub> =2.895, p=0.044	H=55.796	y=539.294, p<0.001
28dpi / contralateral	t <sub>7</sub> =1.032, p=0.336	p<0.001	y=136.188, p>0.05
28dpi / ipsilateral	t <sub>7</sub> =2.894, p=0.023		y=391.984, p<0.001
42dpi / loxP/+	t <sub>4</sub> =0.870, p=0.434	n=9915	y=93.906, p>0.05
42dpi / loxP/loxP	t <sub>4</sub> =3.478, p=0.025	H=87.162	y=693.091, p<0.001
42dpi / contralateral	t <sub>8</sub> =1.040, p=0.329	p<0.001	y=82.049, p>0.05
42dpi / ipsilateral	t <sub>8</sub> =4.059, p=0.004		y=681.234, p<0.001
84dpi / loxP/+	t <sub>6</sub> =1.843, p=0.125	n=7378	y=16.550, p>0.05
84dpi / loxP/loxP	t <sub>3</sub> =8.578, p=0.003	H=52.415	y=466.868, p<0.001
84dpi / contralateral	t <sub>8</sub> =0.682, p=0.515	P<0.001	y=143.428, p>0.05
84dpi / ipsilateral	t <sub>8</sub> =3.495, p=0.008		y=593.745, p<0.001

804

805 Table 2. Results of statistical tests performed for immunohistochemical stainings. Numbers in  
806 subscript in t-tests represent degrees of freedom. D, H and y represent test statistics for  
807 Kolmogorov-Smirnov tests, Kruskal-Wallis tests and Dunn's multiple comparison tests,  
808 respectively.



# Figure 1

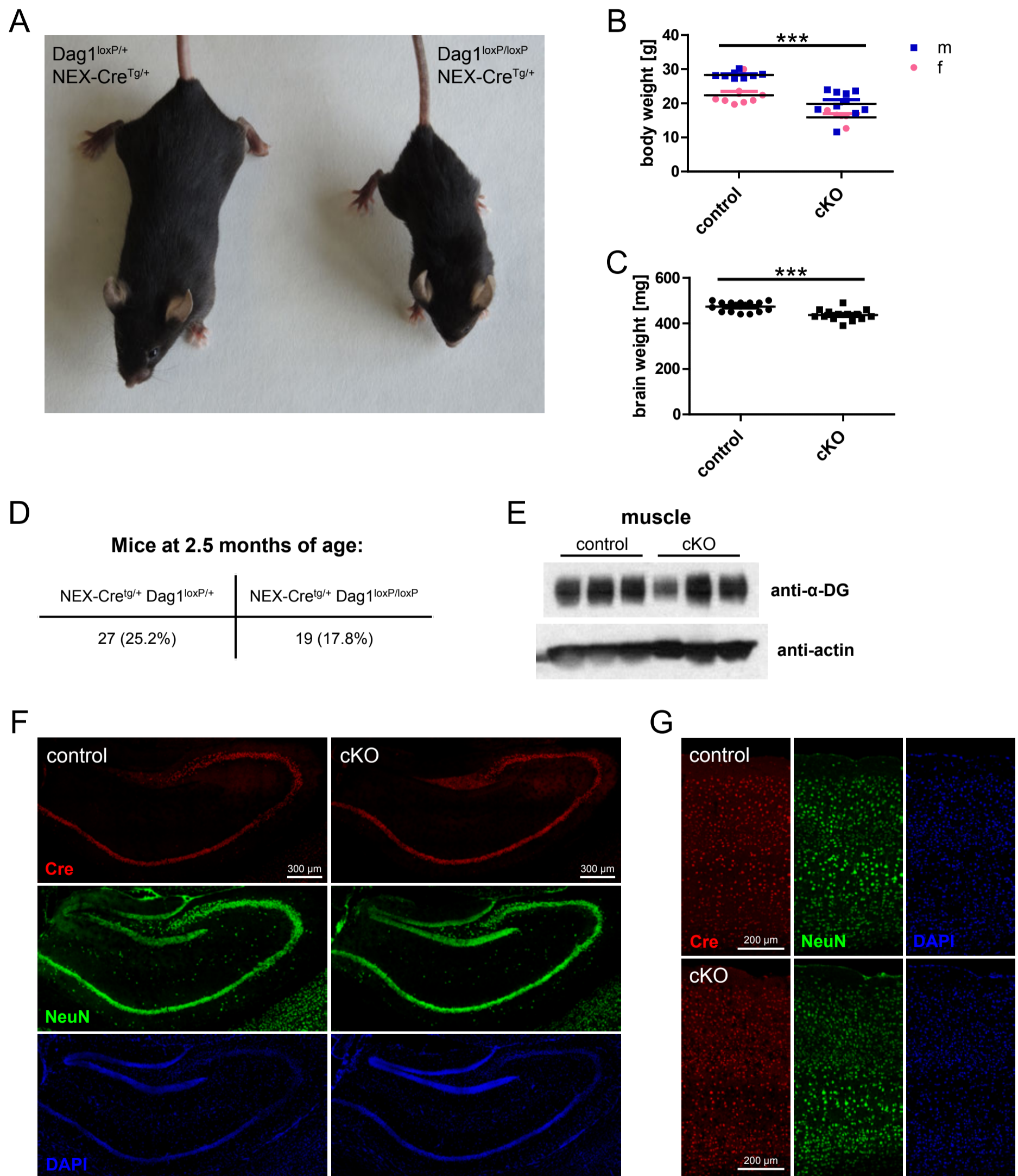
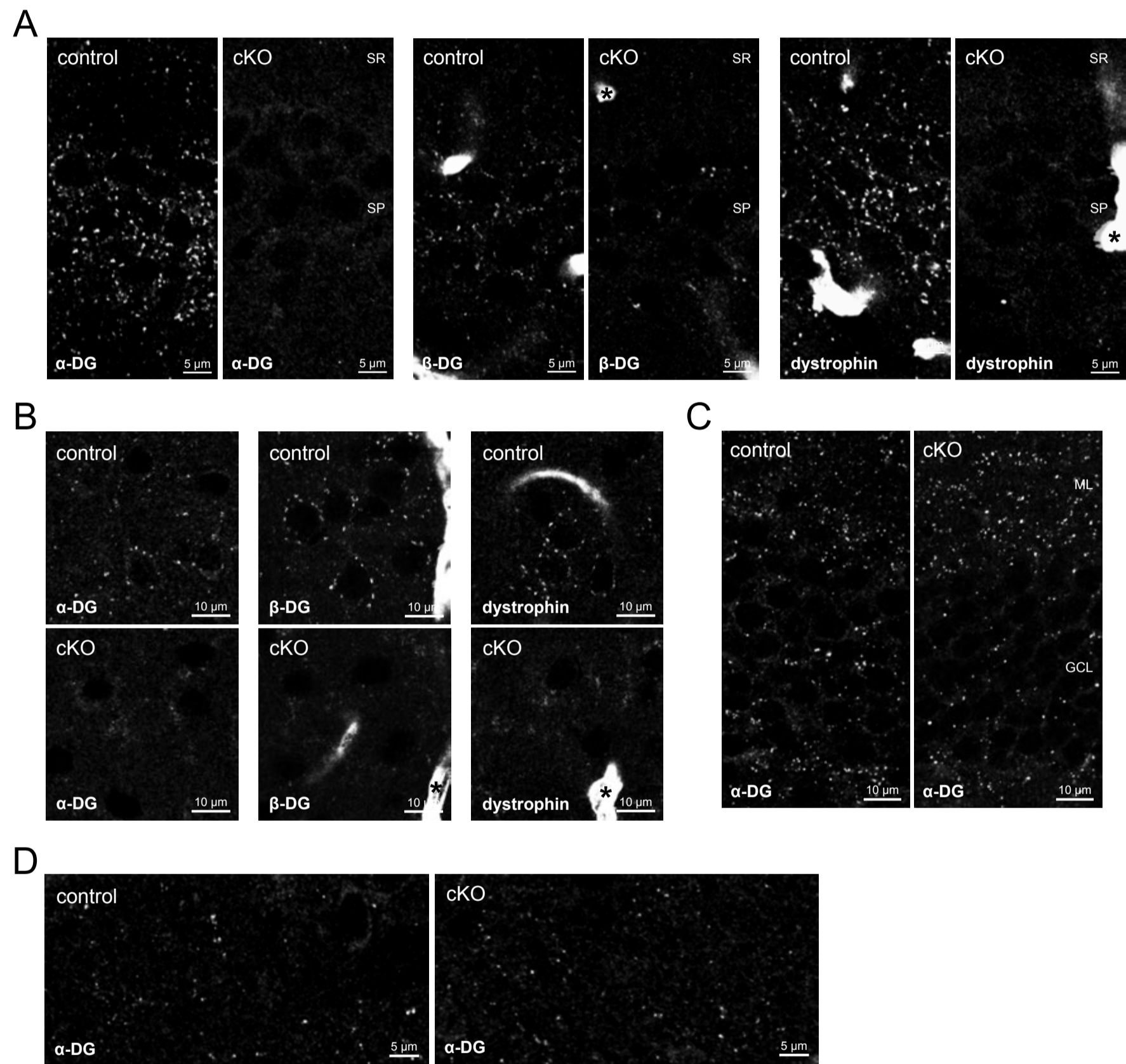
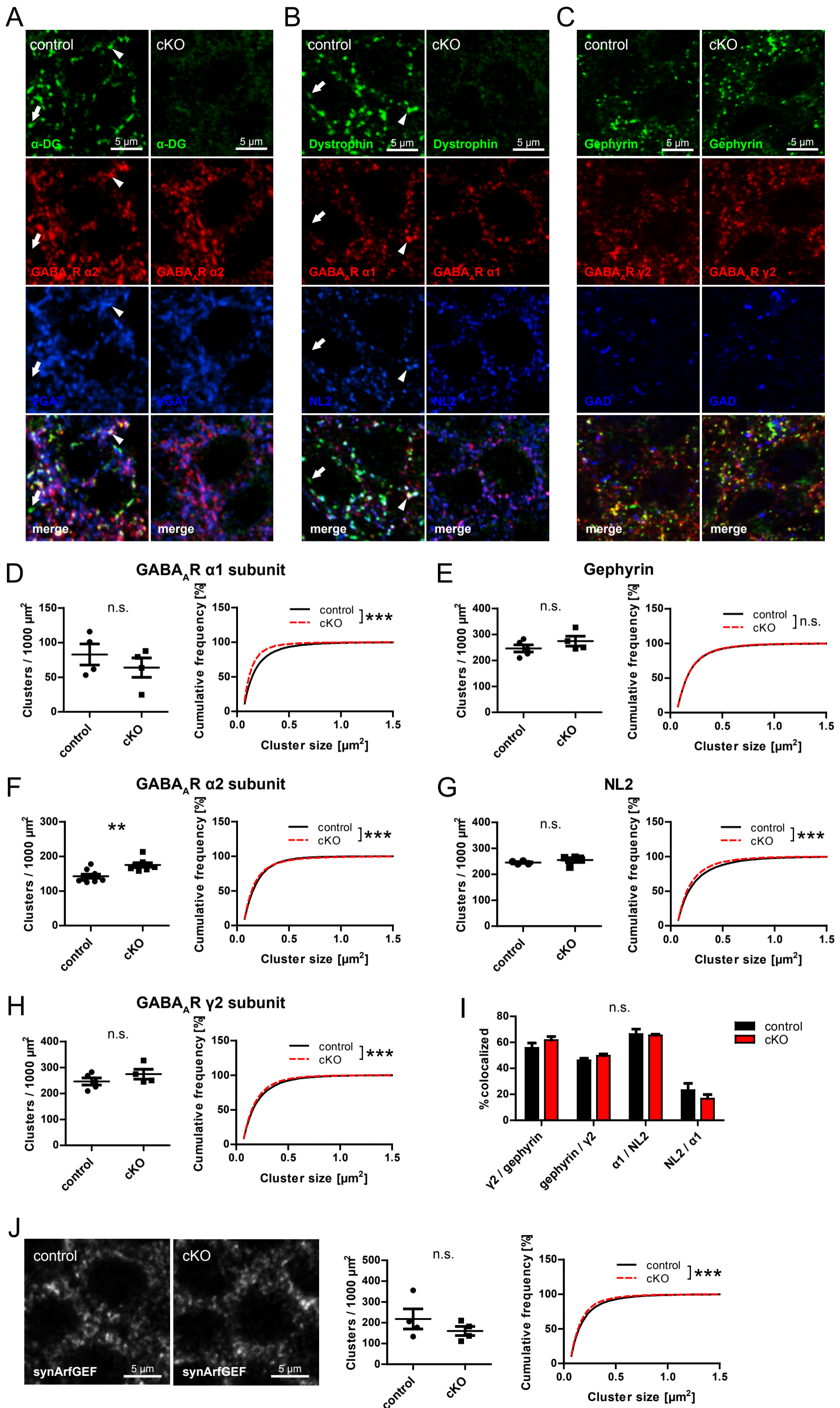


Figure 2





# Figure 3





# Figure 4

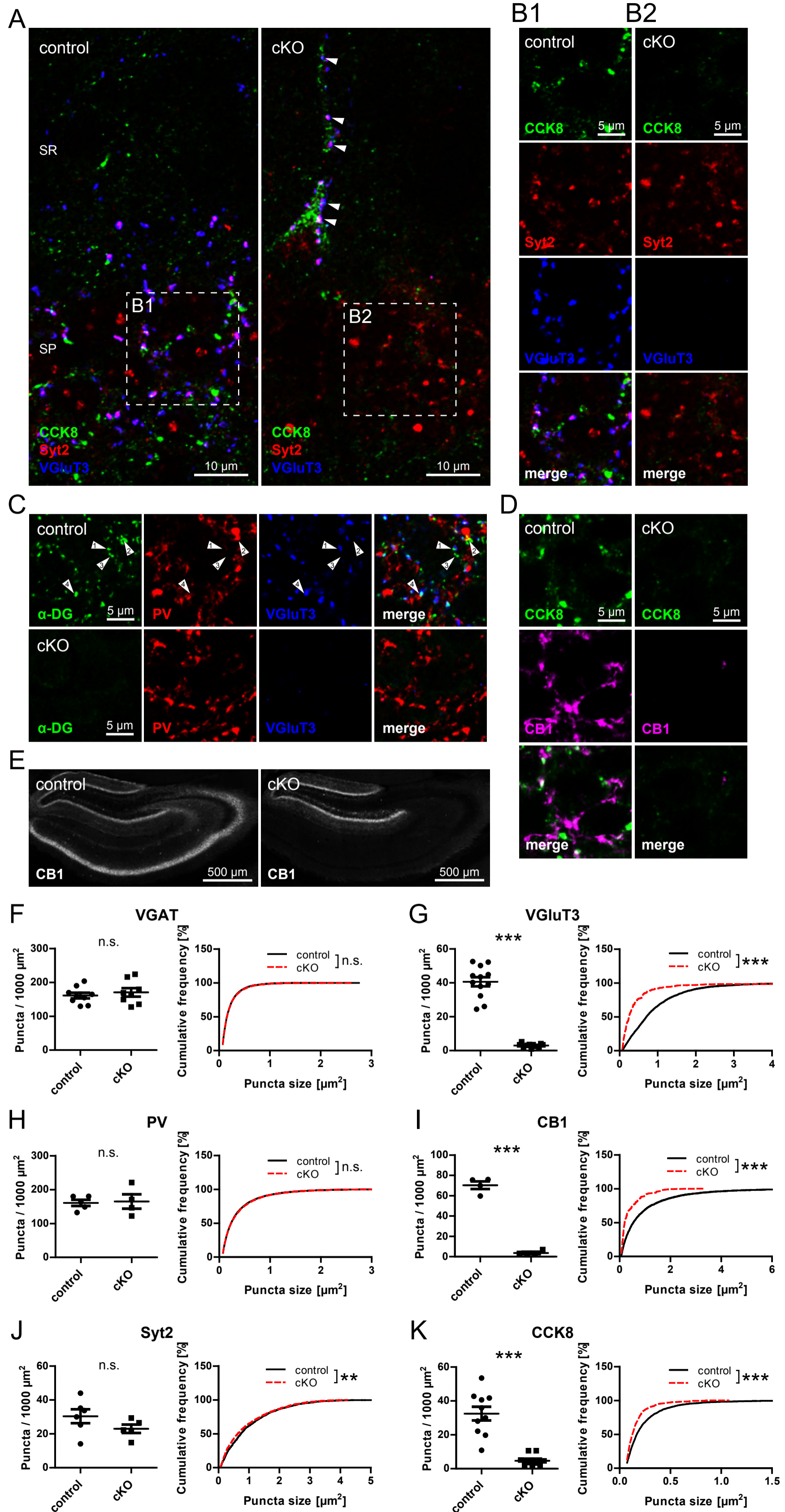


# Figure 5

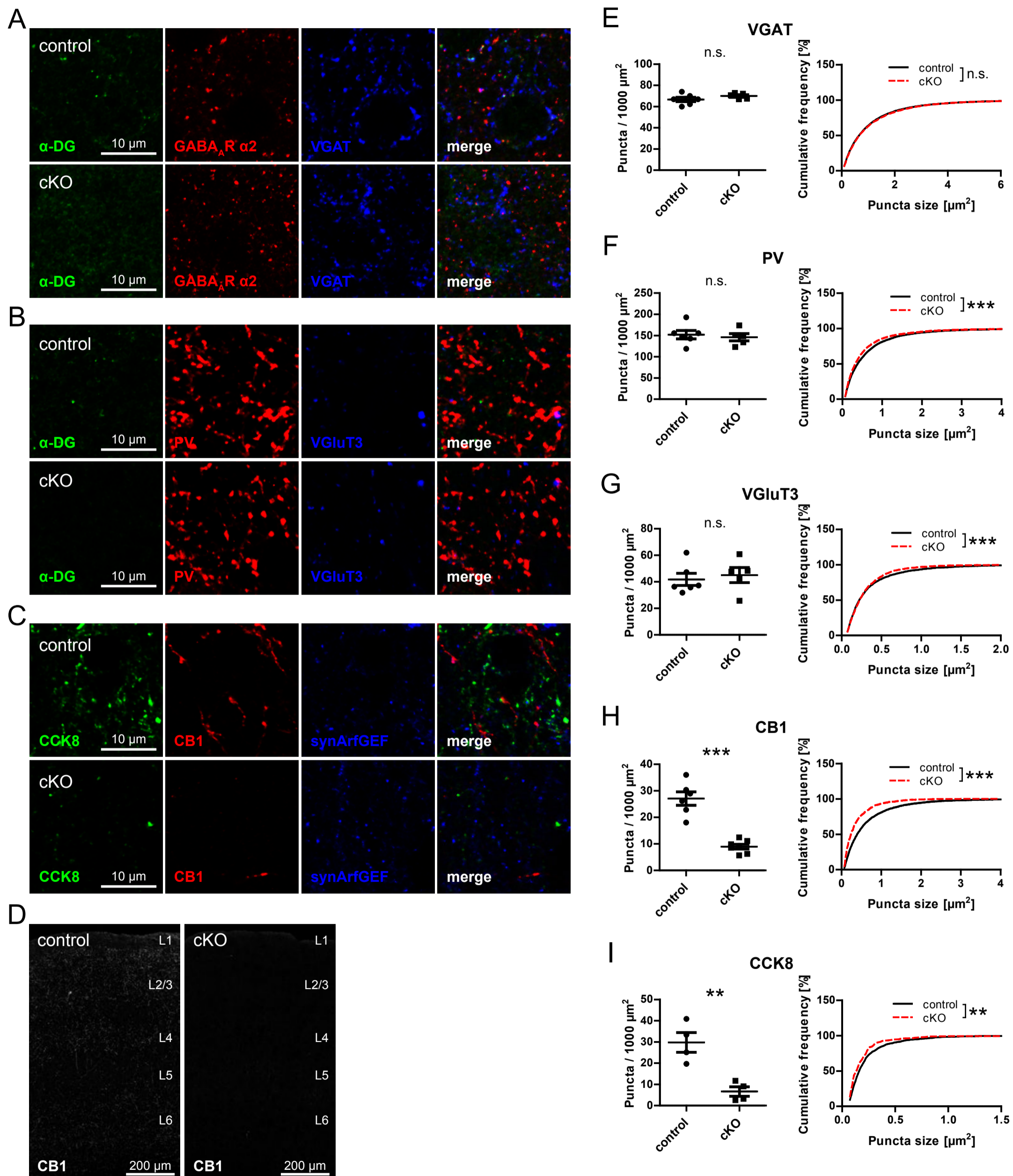




# Figure 6

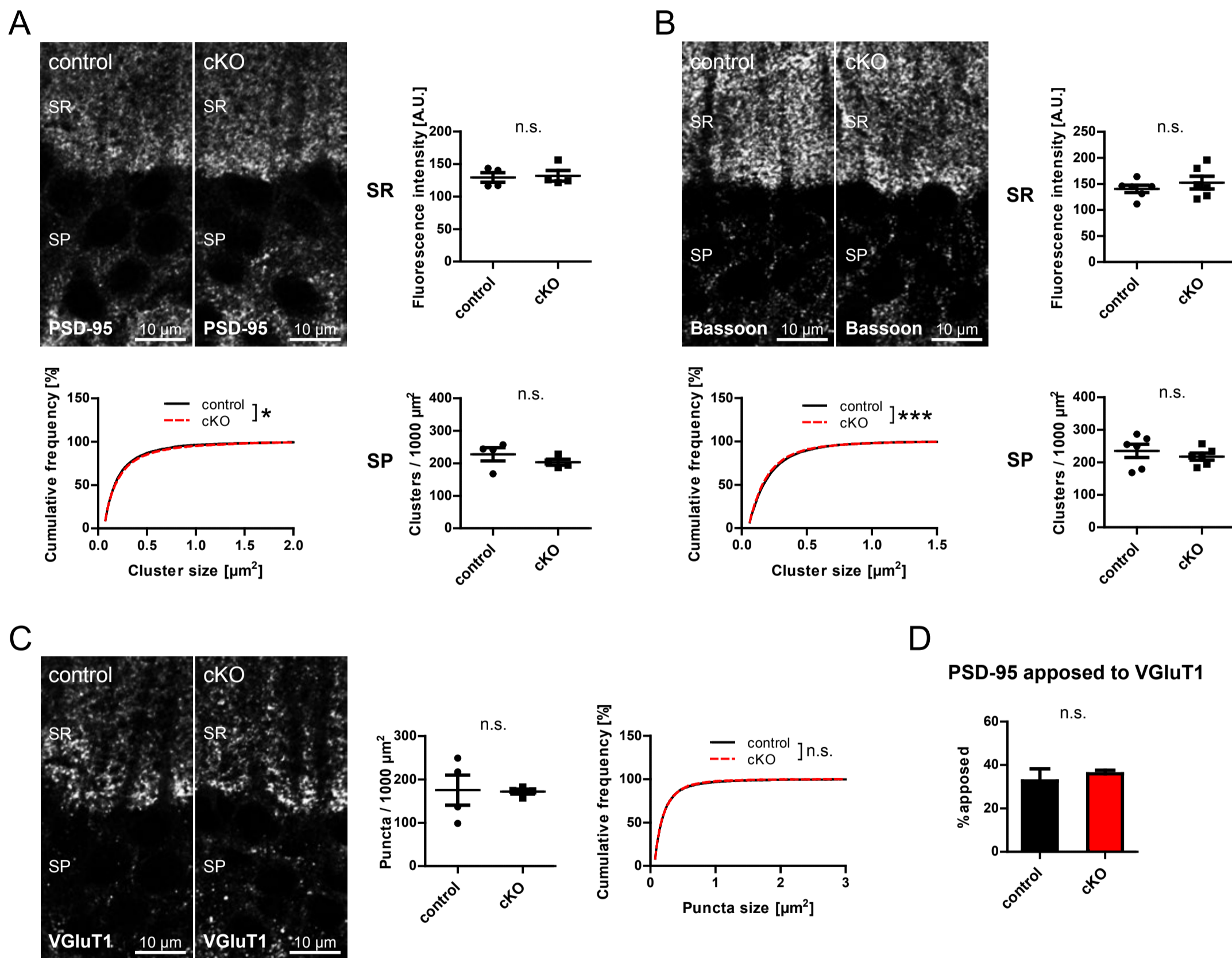
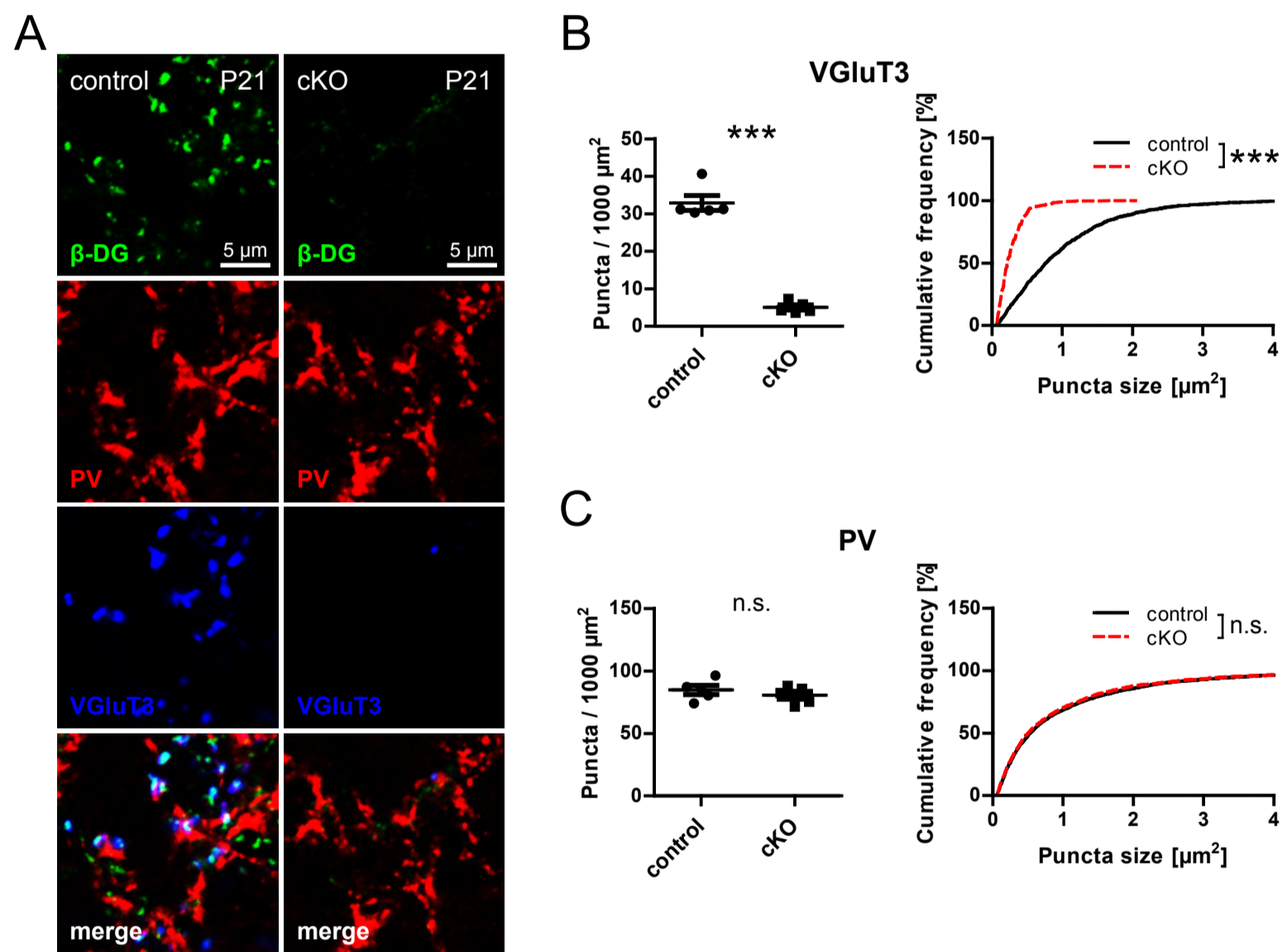
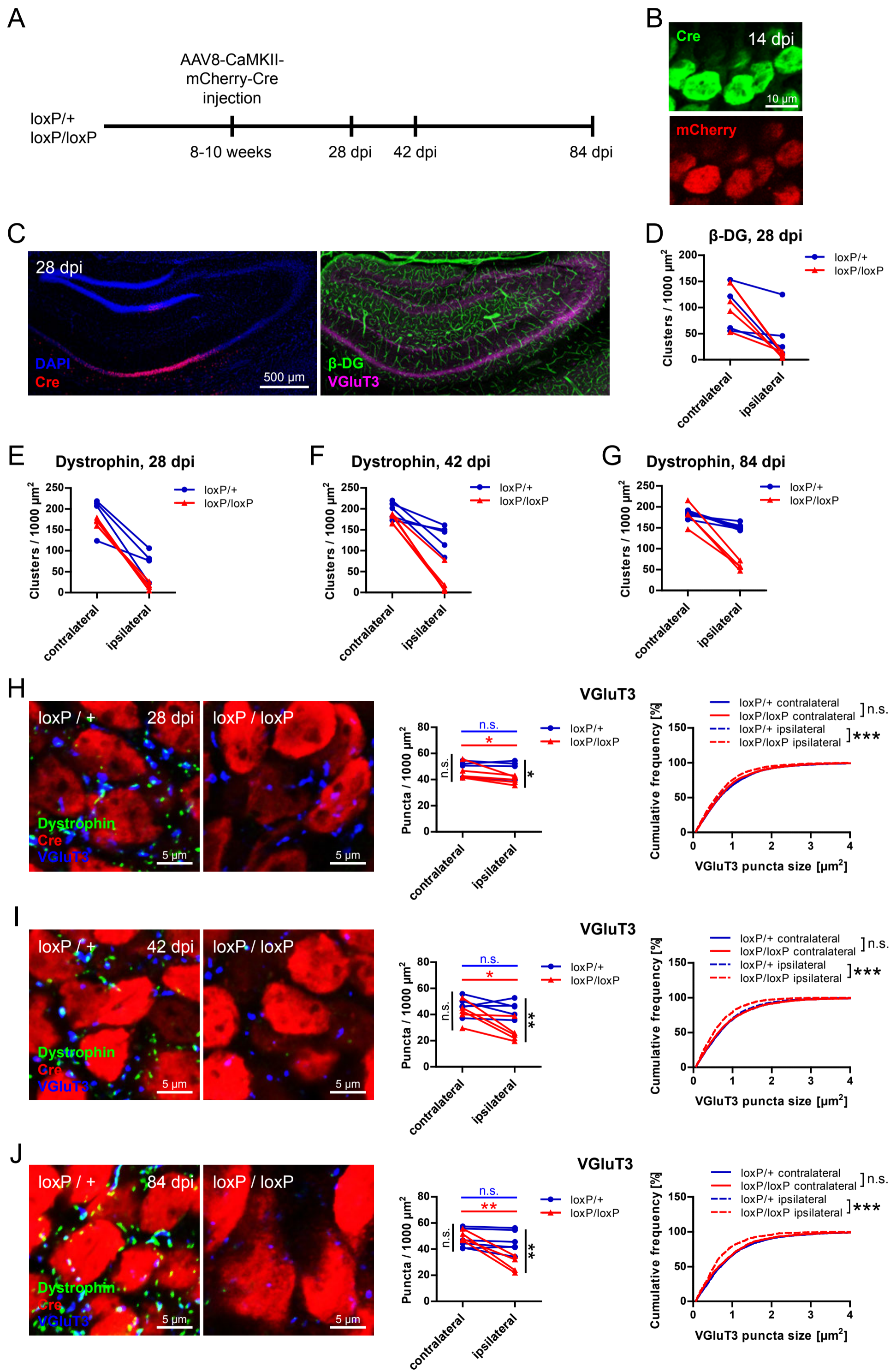


Figure 7



# Figure 8





# Figure 9

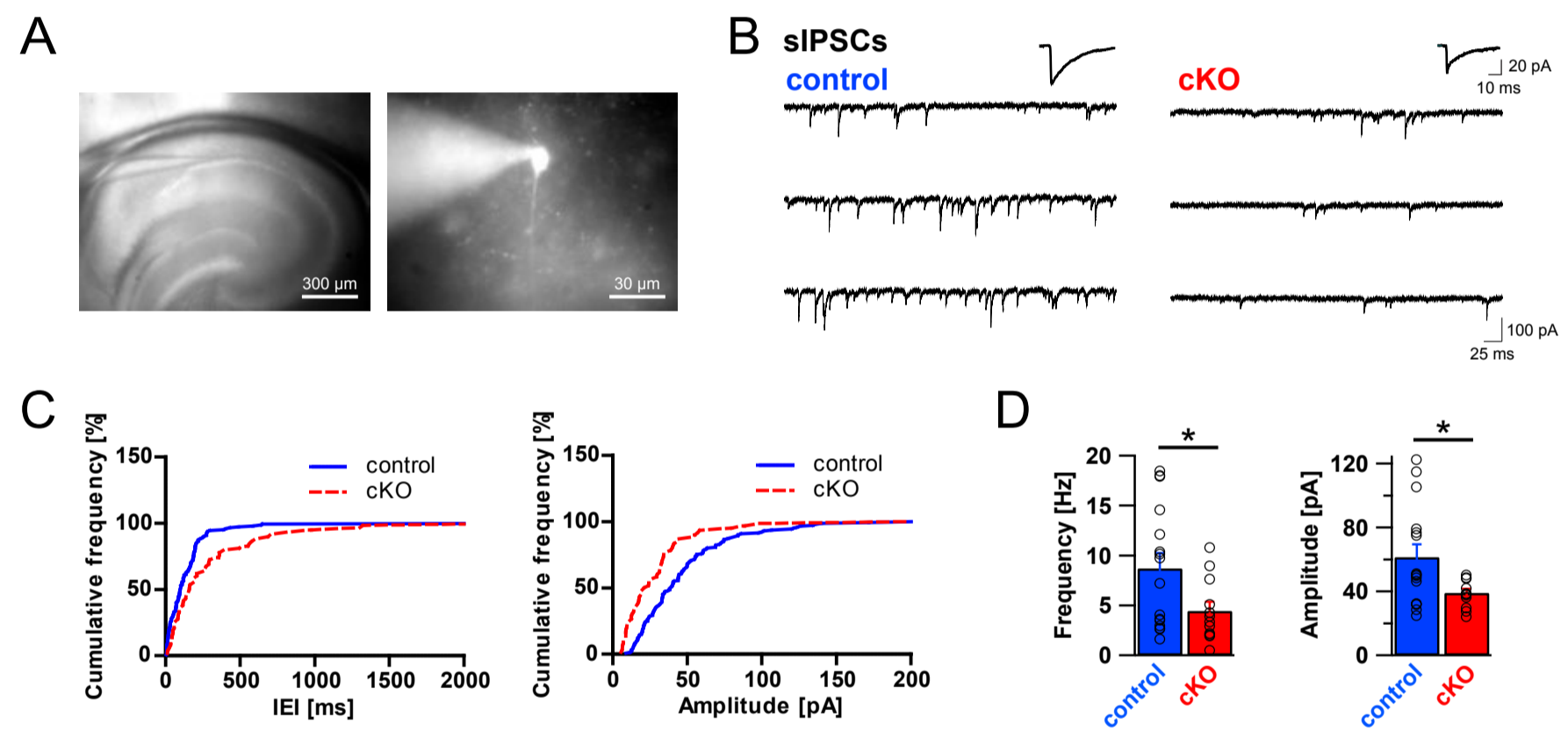


# Figure 10

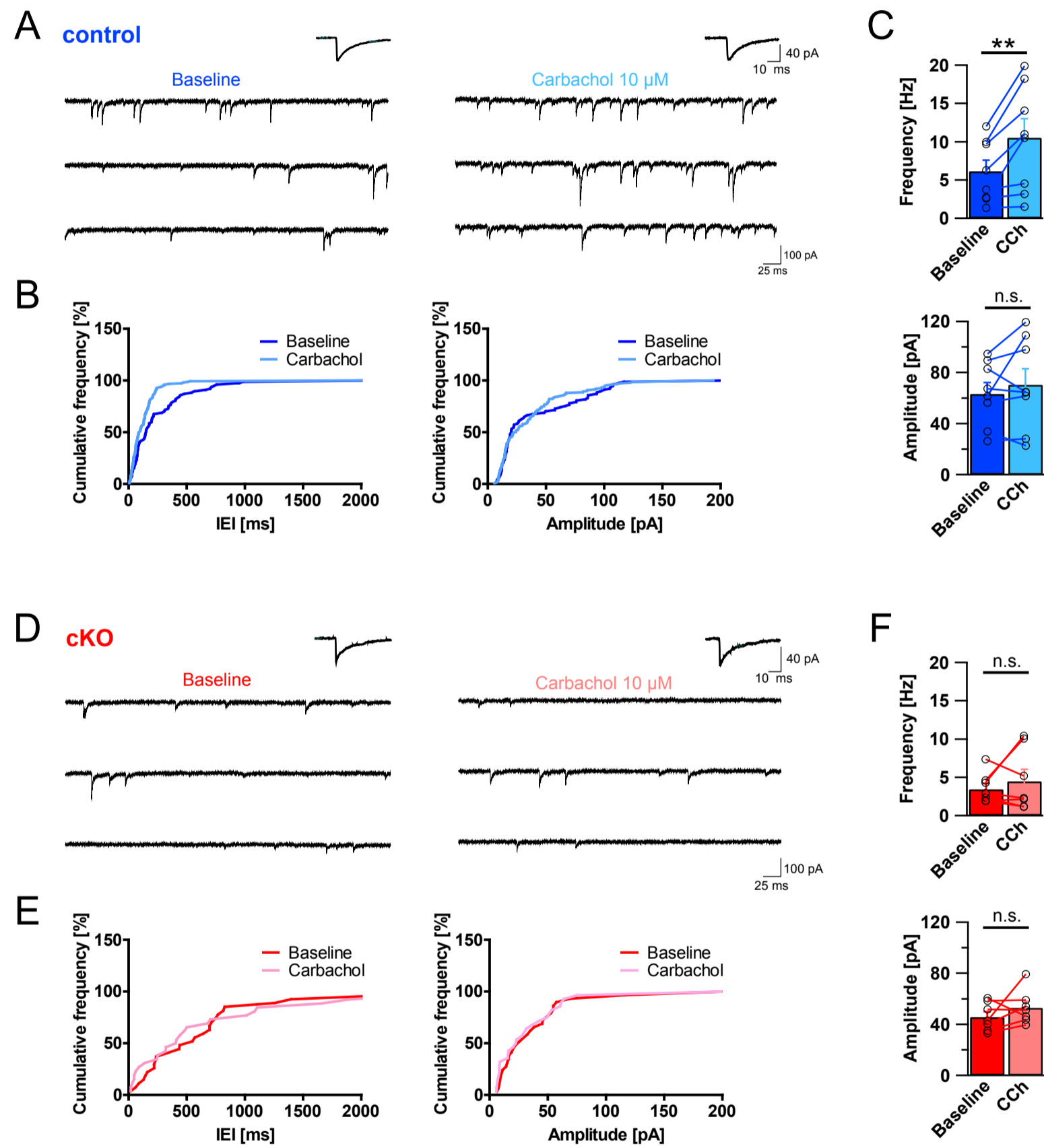


# Figure 11

